SELENOPHENE BEARING BENZODITHIOPHENE BASED ALTERNATING POLYMERS FOR ORGANIC SOLAR CELL APPLICATIONS

A THESIS SUBMITTED TO
THE GRADUATE SCHOOL OF NATURAL AND APPLIED SCIENCES
OF
MIDDLE EAST TECHNICAL UNIVERSITY

BY

GÜLTEN ÖZKUL ATLI

IN PARTIAL FULFILLMENT OF THE REQUIREMENTS
FOR
THE DEGREE OF MASTER OF SCIENCE
IN
CHEMISTRY

DECEMBER 2019

Approval of the thesis:

SELENOPHENE BEARING BENZODITHIOPHENE BASED ALTERNATING POLYMERS FOR ORGANIC SOLAR CELL APPLICATIONS

submitted by **GÜLTEN ÖZKUL ATLI** in partial fulfillment of the requirements for the degree of **Master of Science in Chemistry Department, Middle East Technical University** by,

Prof. Dr. Halil Kalıpçılar
Dean, Graduate School of **Natural and Applied Sciences** _____

Prof. Dr. Cihagir Tanyeli
Head of Department, **Chemistry** _____

Prof. Dr. Ali Çırpan
Supervisor, **Chemistry, METU** _____

Examining Committee Members:

Prof. Dr. Levent Kamil Toppare
Chemistry, Middle East Technical University _____

Prof. Dr. Ali Çırpan
Chemistry, METU _____

Prof. Dr. Yasemin Arslan Udum
Technical Sciences Vocational School, Gazi University _____

Assoc. Prof. Dr. Görkem Emrullah Günbaş
Chemistry, Middle East Technical University _____

Assoc. Prof. Dr. İrem Erel Göktepe
Chemistry, Middle East Technical University _____

Date: 24.12.2019

I hereby declare that all information in this document has been obtained and presented in accordance with academic rules and ethical conduct. I also declare that, as required by these rules and conduct, I have fully cited and referenced all material and results that are not original to this work.

Name, Surname: Gülten Özkul Atlı

Signature:

ABSTRACT

SELENOPHENE BEARING BENZODITHIOPHENE BASED ALTERNATING POLYMERS FOR ORGANIC SOLAR CELL APPLICATIONS

Özkul Atlı, Gülten
Master of Science, Chemistry
Supervisor: Prof. Dr. Ali Çırpan

December 2019, 87 pages

In recent years, copolymers designed by different donor-acceptor (D-A) combinations for high-efficiency photovoltaic applications have been advanced to achieve broad absorption spectra and suitable molecular energy levels. Donor-acceptor design approach in photovoltaic polymers provides easy tuning of optical and electronic features of desired polymers. Moreover, π-bridges utilized in D-A type polymer main chain have been studied extensively to extend π delocalization and conjugation length of well-designed polymer. In this regard, D-A type two copolymers based on benzodithiophene moiety as the electron-rich donor unit and benzotriazole moiety functionalized by alkyl chain as the electron deficient acceptor unit with different π-bridges were designed for organic solar cell applications. Two copolymers P1 and P2 were synthesized via Stille coupling reaction to realize the impacts of structural modifications on electronic and optical features. While P1 has a thiophene π-bridge unit in its backbone, selenophene was utilized as the π-bridge moiety in main chain of P2.

Synthesized polymers P1 and P2 were analyzed by ^{1}H and ^{13}C NMR spectroscopy, TGA, DSC, CV, and UV-Vis-NIR spectroscopy to characterize their structural, electronic and optical properties. Structure of polymers was investigated by Nuclear

Magnetic Resonance Spectroscopy. Highest occupied molecular orbital and lowest unoccupied molecular orbital energy levels and band gap values were determined via cyclic voltammetry and UV-Vis-NIR absorption spectra. Photovoltaic properties were investigated ITO/PEDOT:PSS/Polymer:PCBM/LiF/Al device structure measured under standard AM 1.5 G illumination (100 mW/cm^2). As a consequence of measurements under standard AM 1.5 G illumination (100 mW/cm2), the highest power conversion efficiency values were recorded as 2.41% and 1.56% for P1 and P2 based OSCs, respectively.

Keywords: Benzodithiophene, Benzotriazole, Conjugated Polymers, Organic Solar Cells, Stille Coupling Reaction

ÖZ

ORGANİK GÜNEŞ PİLİ UYGULAMALARI İÇİN SELENOFEN İÇEREN BENZODİTİYOFEN BAZLI SIRALI POLİMERLER

Özkul Atlı, Gülten
Yüksek Lisans, Kimya
Tez Danışmanı: Prof. Dr. Ali Çırpan

Aralık 2019, 87 sayfa

Son yıllarda, yüksek verimli fotovoltaik uygulamalar için geniş soğurma spektrumları ve uygun moleküler enerji seviyeleri elde edebildiğimiz farklı donor-akseptör (D-A) kombinasyonları ile tasarlanan kopolimerler geliştirilmiştir. Fotovoltaik polimerlerde donör-akseptör yaklaşımı, istenen polimerlerin hem optik hem de elektronik özelliklerinin kolayca ayarlanmasını sağlar. Ayrıca, D-A yaklaşımı ile sentezlenen polimerlerin ana zincirlerinde kullanılan π-köprülerinin, polimerlerin π-delokalizasyon sistemlerini ve konjugasyon uzunluklarını geliştirdikleri bu alanda yapılan bir çok çalışma ile desteklenmiştir. Bu bağlamda, benzoditiyofen (BDT) ünitesi elektron bakımından zengin bir donör olarak ve alkil grubu ile fonksiyonlandırılmış benzotrizole (BTz) ünitesi akseptör olarak kullanılan, farklı π-köprülere sahip iki D-A tipi konjüge kopolimer organik güneş pili uygulamaları için tasarlandı. Yapısal modifikasyonların elektronik ve optik özellikler üzerindeki etkilerini gerçekleştirmek için farklı π-köprü üniteli iki kopolimer P1 ve P2 Stille kenetlenme reaksiyonu ile sentezlendi. P1'in omurgasında π-köprü ünitesi olarak tiyofen grubu kullanılırken, P2'nin ana zincirinde π-köprüsü olarak selenofen kullanıldı.

Sentezlenen Pl ve P2 polimerlerinin, yapısal, elektronik ve optik özelliklerini karakterize etmek için ^{1}H ve ^{13}C NMR spektroskopisi, TGA, DSC, CV ve UV-Vis-

NIR spektroskopisi kullanıldı. Polimerlerin yapısal özellikleri Nükleer Manyetik Rezonans Spektroskopisi ile incelendi. En yüksek dolu moleküler orbital ve en düşük boş moleküler orbital enerji seviyeleri ve bant aralığı değerleri, siklik voltammetri ve UV-Vis-NIR soğurma spektrumu ile belirlendi. Fotovoltaik özellikler, standart AM 1.5 G aydınlatma (100 mW/cm^2) altında ölçülen ITO/PEDOT: PSS/Polimer:PCBM/LiF/Al cihaz yapısı incelendi. P1 ve P2 bazlı organik güneş gözeleri için maksimum güç dönüşüm verimi değerleri sırasıyla %2.41 ve %1.56 olarak kayıtlara geçmiştir.

Anahtar Kelimeler: Benzoditiyofen, Benzotriazol, Konjüge Polimerler, Organik Güneş Pilleri, Stille Kenetlenme Reaksiyonu

To my beloved family…

ACKNOWLEDGEMENTS

First of all, I would like to special thank my supervisor Prof. Dr. Ali Çırpan for the opportunity he gave me to work in his research group, his endless support, guidance, and patience throughout my thesis study. He showed me that a good leader can always find the positive side, no matter the situation.

I am grateful to Prof. Dr. Levent Toppare for his scientific support and guidance. I owe him gratitude for his scientific cooperation and contributions to my thesis study.

I would like to thank Prof. Dr. Yasemin Arslan Udum and Hatice Sarıgül for their endless help in the electrochemical characterizations. I would like to thank to Eda Alemdar Yılmaz for her endless help in the photovoltaic studies.

I am extremely grateful to Sultan Aslan Taşkaya for her precious guidance, support and patience during the whole my master study.

Special thanks to my precious friend Meriç Çalışkan for every moment we spent together. There are no words to explain the value of her friendship for me. Wherever I go, you will remain my best friend.

I would like to thank my friends Mert Can Erer and Merve Yıldırım for their friendships, encouragements and especially their tolerance not only during my happy times but also during the times I felt collapsed. I will always be there whenever they need me.

I owe a dept of gratitude for my lovely lab mates Berrin, Yeşim, Ali Sait, Oğuzhan, Dilan Ece, Selin and Yeliz for their friendships, supports, helps and providing perfect work environment. I will miss our working times and happy coffee breaks.

I would like to present my deepest thank to Hasan Atlı for his endless and unconditional love. I am gratefull for him to be there for me every moment I need him.

The last but definitely not the least, I would special thank my precious family for their unconditional love, care and tolerance. Without their support, I do not think that I could overcome the difficulties during these years.

TABLE OF CONTENTS

LIST OF TABLES

TABLES

LIST OF FIGURES

FIGURES

LIST OF ABBREVIATIONS

ABBREVIATIONS

ACN	Acetonitrile
AFM	Atomic force microscopy
Ag	Silver
Al	Aluminum
AM1.5G	Air mass 1.5 global
BDT	Benzodithiophene
BHJ	Bulk heterojunction
BLA	Bond length alternation
BTz	Benzotriazole
CB	Conduction band
$CDCl_3$	Chloroform
CE	Counter electrode
CP	Conjugated polymer
CV	Cyclic voltammetry
D-A	Donor-Acceptor
DCB	1,2-dichlorobenzene
DIO	1,8-diiodooctane
DPE	Diphenyl ether
DSC	Differential scanning calorimetry

EC	Electrochromic
ECD	Electrochromic device
E_g	Band gap
E_g^{el}	Electronic band gap
E_g^{op}	Optical band gap
EQE	External quantum efficiency
ETL	Electron transport layer
eV	Electron volt
FF	Fill factor
GPC	Gel permeation chromatography
HOMO	Highest occupied molecular orbital
HTL	Hole transport layer
ICT	Intramolecular charge transfer
ITO	Indium tin oxide
J_{max}	Maximum current density
J_{sc}	Short circuit current density
J-V	Current Density-Voltage
LiF	Lithium fluoride
LUMO	Lowest unoccupied molecular orbital
NIR	Near infrared
OFET	Organic field effect transistor
OLED	Organic light emitting diode

OPV	Organic photovoltaic
OSC	Organic solar cell
PA	Polyacetylene
PANI	Polyaniline
$PC_{71}BM$	Phenyl-C71-butyric acid methyl ester
PCE	Power conversion efficiency
PDI	polydispersity index
PEDOT	polyethylenedioxythiophene
PEDOT:PSS	Poly(3,4-ethylenedioxythiophene)-Polystyrenesulfonate
P_{in}	Incident light power
P_{max}	Maximum power
PPP	Polyparaphenylene
PPy	Polypyrrole
PT	Polythiophene
Pt	Platinum
RE	Reference electrode
R_s	Series resistance
R_{sh}	Shunt resistance
SHE	Standard hydrogen electrode
$TBAPF_6$	Tetrabutylammonium hexafluorophosphate
TGA	Thermogravimetric analysis
THF	Tetrahydrofuran

UV-Vis	Ultraviolet-visible
VB	Valance band
V_{max}	Maximum voltage
V_{oc}	Open circuit voltage
WE	Working electrode
WO_3	Tungsten trioxide

CHAPTER 1

INTRODUCTION

1.1. Conjugated Polymers

Polymer is simply described as a very large molecule composed of many small particles bonded by the covalent bond in several ways. Polymers were formerly considered as insulator materials. In fact, people used polymers to coat electric wires to protect themselves from short circuits [1]. This traditional concept was changed with the great discovery of polyacetylene as a conductor -after the doping process via oxidation- in 1977 by Hideki Shirakawa, Alan Macdiarmid, and Allan Heeger. Owing to this pioneering discovery, those scientists received the 2000 Nobel Prize in the field of chemistry. Immediately after the epochal discovery of doped polyacetylene exhibited conductive properties, a series of conductive polymers were developed and recorded [2]. After these discoveries, studies on fields of electronics and photonics gained vital interests due to the excellent optical and semiconducting properties of conjugated polymers [3].

Organic conjugated polymers are mainly organic compounds that possess the ability to conduct electricity. Significant characteristics of conducting electricity results from their intrinsic property that have alternating single and double bond in polymer backbones where their extended p-orbital system creates electrons can delocalize through whole polymer chain [4]. Polyacetylene (PA), polythiophene (PT), polypyrrole (PPy), polyethylenedioxythiophene (PEDOT), and polyparaphenylene (PPP) are exemplified as some commonly used conjugated polymers. Their molecular structures of main chains were demonstrated in Figure 1.1.

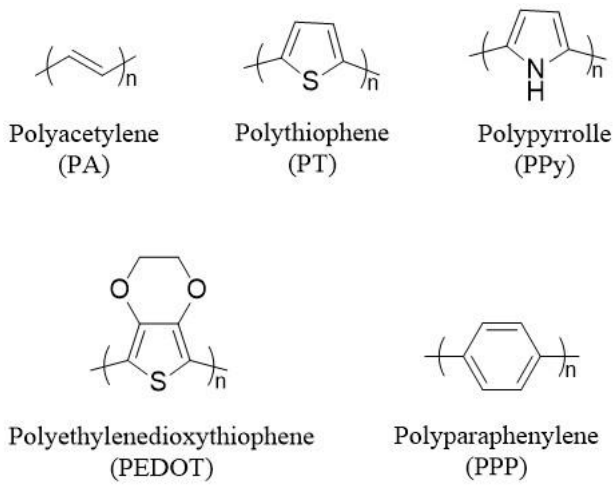

Figure 1.1. Main chain structures of some commonly used CPs

Organic conjugated polymers have drawn spectacular interest thanks to their unique characteristics such as low-cost production, favorable flexibility, lightweight, ease of processability and tunability compared to the inorganic materials and other small molecule semiconductors [5]. These prominent properties are made conjugated polymers appropriate for a broad range of applications such as electrochromic devices, sensors, OLED's, rechargeable batteries, supercapacitors, and photovoltaic cells [6].

1.1.1. Doping Process

In the conjugated polymer system, electron delocalization is formed as a result of the existence of conjugated double bonds in the main chain of polymers. In order to make conjugated polymers conductive materials, introducing mobile charge carriers to double bonds is a necessity [7]. This process is performed by oxidation and/or reduction reactions, which is called doping process. In other words, the process in which π- conjugated polymers are turned from having a very high band gap to a lower band gap is called the doping process [8].

The term 'p-doping' is defined as electrons are removed from HOMO of the conjugated polymers by oxidizing agents such as Br_2, I_2, and AsF_5. The process in

which electrons are donated to LUMO of the conjugated polymers by reducing agents such as Na, Li, and K is called as ‘n-doping’ [9].

As a result of the doping process, specific charge defects which include soliton, polaron, and bipolaron are generated. Mostly, soliton is formed in linear conjugated polymers like polyacetylene (PA) to assist charge transport. Based upon types of redox reactions applied, soliton can occur with a positive or negative charge. The representation of neutral, positive, and negative solitons occur in trans-polyacetylene was depicted in Figure 1.2.

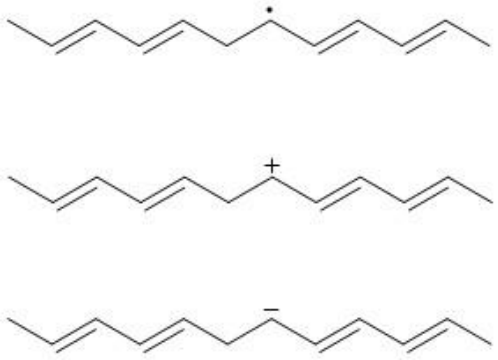

Figure 1.2. Representation of solitons in trans-polyacetylene

In non-degenerated conjugated polymer systems, charge defects, which are polarons and bipolarons, lead charge carriers. Polaron, which can be either radical anion or radical cation is formed by ionization of polymers when heterocyclic compounds are polymerized. In addition, bipolaron can be formed by further ionization [10]. The positive polaron and bipolaron generation in polypyrrole was shown in Figure 1.3.

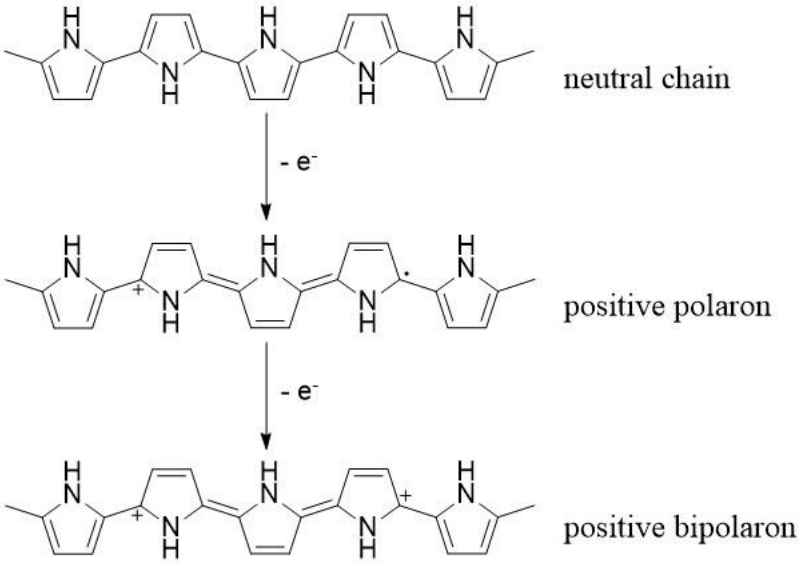

Figure 1.3. Polaron and bipolaron generation in polypyrrole

The doping process has a significant effect on increasing the electrical conductivity of conjugated polymers. Therefore, deciding appropriate methods to achieve high electrical conductivity as a result of the doping process is a critical point. The doping process can be achieved mostly by two main methods, which are chemical and electrochemical. Chemical doping mechanism involves that conjugated polymers are exposed to vapors of oxidizing or reducing agents while the electrochemical doping process consists that thin film of conjugated polymers is oxidized or reduced by applying proper voltage [11].

1.2. Band Theory

With respect to electric conductivity, materials are categorized into three groups, which are metals, semiconductors, and insulators. Their electrical conductivity properties are closely related to the band gaps. The energy distance from the valance band (VB) to the conduction band (CB) is termed as a band gap. While the valence band represents the highest occupied band of electrons, the conduction band states the lowest unoccupied band of electrons [12]. In other words, the band gap is defined as

the minimum energy that is needed to excite an electron from valance band to the conduction band [13].

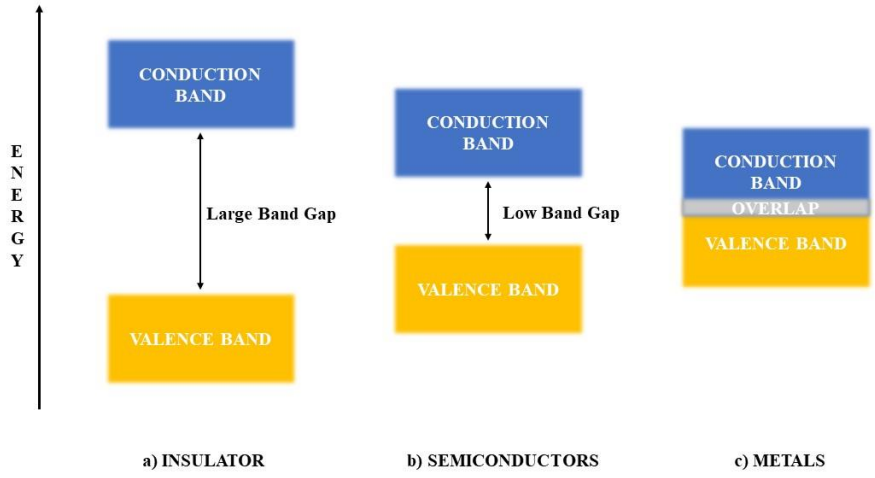

Figure 1.4. General representation of band gap energies for a) insulators, b) semiconductors and c) metals

For the insulative, semiconductive, and conductive materials, dissimilarities in the general size of band gaps were illustrated in Figure 1.4. Depending on the size of band gaps, materials acquire some specific properties.

For insulators, there is a broad band gap between the valance band and conduction band. This large energy gap basically indicates that there is a large forbidden gap between VB and CB that results in preventing electrons jump from VB to CB and also preventing electrons participate in conduction. This explanation provides reasons behind why insulators could not conduct electricity well. Their band gap is too large in order that electrons can obtain adequate energy to reach the conduction band thus, insulators could not conduct electricity.

For conductors, there is an overlap between the valance band and conduction band. Unlike insulators, this overlap provides that electrons in the valance band are able to move freely in the conduction band and also participate in conduction easily.

For semiconductors, there is enough band gap between the valance band and conduction band in order that electron can jump from VB to CB. Generally, their band gaps are between insulators and conductors with respect to their sizes. Although a finite amount of electrons could jump to conduction band resulting in conducting electricity slightly. This excitation of electrons enables to function as achieving extra conduction process due to the formation of electron holes. By occupying these electron holes with electrons from atom next to it, chain reactions of holes and electrons are created that results in generating current. The conductivity of semiconductor materials can be increased by doping materials in small quantities [14]–[16].

1.2.1. Structural Band Gap Tuning in Conjugated Polymers

From the point of compelling challenges and complicated prerequisites of conjugated polymers design for the photovoltaic applications, well-tuning the band gap process is essential importance [14]. Effective tuning band gaps and molecular structures of conjugated polymers highly determine their optoelectronic properties to facilitate the major targets and application demands. One of the most crucial requirements of conjugated polymers for organic photovoltaic applications is having a high absorption coefficient in the broad range of the visible region. This requirement can be achieved by decreasing the band gap [17].

There are five main structural factors that designate the band gap of semiconducting conjugated polymers, which are bond length alternation (E_{BLA}), mean deviation from planarity (E_{θ}), aromatic resonance energy (E_{Res}), substitution (E_{Sub}) and intermolecular interactions (E_{Int}). Therefore, the band gap of the conjugated system is stated as:

$$E_g = E_{BLA} + E_{Res} + E_{Sub} + E_{\theta} + E_{Int}$$

For the ground state of π-conjugated systems, two possible resonance forms, which are aromatic and quinoid structures, are presented. An aromatic resonance structure is originated from confined π-electrons, which sustain the aromaticity, while quinoid resonance structure is formed by the delocalization of π-electrons through the conjugation, which converts single bond into double bond and double bond into a single bond. Quinoid form is less energetically stable compared to aromatic structure; thus, it has a smaller band gap. In π-conjugated systems, the ratio between aromatic and quinoid populations can be related to the bond length alternation which is basically explained as the approximate distance between the neighbor carbon-carbon bonds in the polymer chain. It is a significant geometric factor to tune the band gap of semiconductors. BLA value increases when the more aromatic rings exist in the ground state. In other words, when a more quinoid structure exists in the ground state, BLA value decreases, and it results in a narrower band gap.

As mentioned before, aromaticity confines the electrons on the conjugated structure, which results in prevention of π-electron delocalization in structure. This prevention causes to decrease in the mobility of electrons on the polymer backbone. It leads to distortion in conjugation length. Therefore, increasing aromaticity creates the widener band gap of the conjugated polymer.

Another way of the tuning band gap of the conjugated polymers is the introduction of the electron-donating groups and the electron-withdrawing groups into the main chain of the polymer, which is the most straightforward way to regulate the energy levels of both HOMO and LUMO, and therefore E_g. Generally, introducing the electron-withdrawing substituent increases both electron affinity and ionization potential that result in decreasing the LUMO energy level. On the contrary, introducing the electron-donating substituent increases the energy level of HOMO and therefore reduces the resulting energy gap.

Planarization occurs by anchoring the rigid building blocks, which causes reducing the torsion angle between two aromatic units. It leads to extend conjugation length. Thus band gap of conjugated polymers decreases.

Another critical factor that affects the band gap of semiconducting conjugated polymers is intermolecular interaction. In solid-state, molecular packing has an excellent effect on π- π stacking compared to the solution state where polymer chains rotate freely. In other words, solid-state materials have a highly ordered structure and high crystallinity, which causes lower the band gap since it provides enhancement in π-π stacking and charge mobility in comparison with the materials in the solution state [13], [17].

1.3. Donor-Acceptor Approach in Conjugated Polymer Design

The most substantial parameters to specify the optoelectronic characteristics of conjugated polymers are their magnitude of the band gap and locations of HOMO and LUMO energy levels. These two crucial parameters profoundly affect the photovoltaic performance of conjugated polymers. Low band gap polymers that are able to absorb the wider scale of the solar spectrum, particularly absorb photons in the near-IR region, are required to achieve high-performance organic solar cell applications. The most widespread strategy of designing conjugated polymers with a narrow band gap is the donor-acceptor (D-A) approach that includes repeatedly alternating conjugated donor (D) moiety and conjugated acceptor (A) moiety introduced in the same main chain of polymer [18]. The term donor-acceptor (D-A) approach for the conjugated polymer design was presented the first time by Havinga and co-workers in 1992 [19].

This unique approach involves creating new energy levels of HOMO and LUMO when interactions are take placed along the both HOMO and LUMO of donor and acceptor moieties of D-A type polymer. These generated new hybridized molecular orbitals that result in higher energy level HOMO and lower energy level LUMO lead to narrower band gap and decreasing E_g^{opt} [13]. Illustration of new energy levels and resulting new band gap for D-A type polymer was illustrated in Figure 1.5.

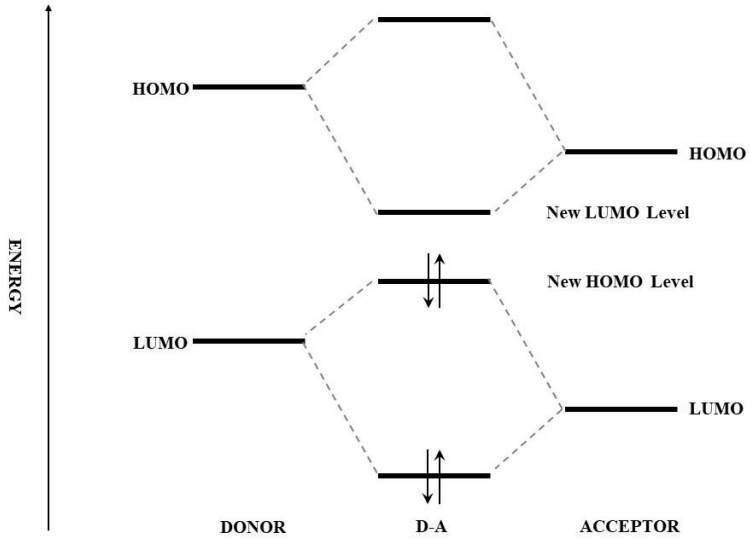

Figure 1.5. Generation of new HOMO-LUMO energy levels in donor-acceptor approach

The most determinant factor tune the band gap is the proper choice of donor and acceptor moieties among the main chain of polymer. This polymer design strategy can be used to control the essential parameters of photovoltaic devices such as Voc and Jsc in order to achieve high PCEs in PSC devices.

1.4. Monomer Moieties in Donor-Acceptor Type Conjugated Polymers

1.4.1. Benzodithiophene Moiety

Benzodithiophene (BDT) has a symmetric and planar structure that comprises of benzene ring with fused thiophenes. It is commonly used as high-performance donor moiety for copolymers that designed and synthesized for photovoltaic applications. Its planar and symmetric structure that leads to increasing the π-π stacking of the polymer provides that BDT-containing copolymers possess high hole mobility and appropriate electronic energy levels. In 2008, Hou and coworkers first presented benzodithiophene based polymer for the photovoltaic applications and investigated that optical and

electronic properties of the polymers containing BDT moiety could be regulated quite easily. Therefore, BDT moiety became an attractive molecule for π-conjugated polymers that used in photovoltaic applications [20], [21]. In addition to these, various types of substituents can be attached easily on the BDT unit in order to increase solubility and regulate the energy levels of polymers. The structure of benzodithiophene was illustrated in Figure 1.6.

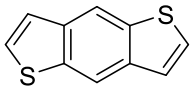

Figure 1.6. Structure of benzodithiophene

1.4.2. Benzotriazole Moiety

Benzotriazole (BTz) is a moderately electron deficient molecule due to its diimine structure, and also could be modified by attaching alkyl groups to enhance solubility at one of the nitrogen atoms. This structural advantage makes it a desirable molecule for obtaining high solution-processable polymers. BTz based polymers are easily synthesized compared to other derivatives. Since they have favorable structural functionalization positions that are easily modified, BTz based polymers are used for various kinds of applications such as ECDs, OPVs, OFET, and OLEDs [22]–[25]. The structure of the benzotriazole unit was demonstrated in Figure 1.7.

Figure *1.7*. Structure of benzotriazole

1.4.3. π-Bridges: Thiophene and Selenophene Moieties

The π-bridge on the polymer main chain substantially affects the parameters for achieving high-efficient photovoltaic applications such as electronic/optical/ electrochemical properties of polymer and interactions between donor and acceptor moiety in polymer backbone [26]. In addition to these, π-bridge is attached between the donor and acceptor moieties in order to provide decreasing the steric hindrance that occurred between D-A units and also enhancing the planarity of the polymer main chain [27].

Thiophene is one of the most commonly used molecules as a π-bridge to connect donor and acceptor moieties of polymers since it has high charge transport ability in the polymer backbone and also extends the conjugation length of the polymer. In addition to these, thiophene as a π-bridge provides widening the absorption in the direction of NIR wavelengths besides increasing the absorption coefficient because of providing strong intramolecular charge transfer (ICT) [28].

Selenophene which is an analog of thiophene where the sulfur atom is altered by selenium atom can be used as a π-bridge to connect donor and acceptor moieties in polymer main chain. It has some advantages over the thiophene unit in photovoltaic applications. Selenophene has lower aromaticity than thiophene since selenium is larger than sulfur with respect to their size and therefore, selenium orbitals cause poor overlap with the π-system of carbon frame. As a result of these, selenophene has more quinoidal character that results in increasing conjugation length of polymers more than thiophene provides and observing the red shift in the absorption spectrum. Moreover, the selenium atom is more polarizable than a sulfur atom that results in promoting Se-Se intermolecular interactions, and thus it enhances the charge carrier mobility [29]. Structures of selenophene and thiophene was illustrated in Figure 1.8.

Figure *1.8*. Structures of thiophene and selenophene

1.5. Electrochromism

The term chromism is described as a change occurring reversibly in substance color that results from applied specific stimulus on it. Materials that show these kinds of features are called chromic materials. There are different kinds of chromic materials such as inorganic, organic, and polymeric. Depends on the mechanism of stimulus, chromism is categorized as photochromism, halochromism, thermochromism, piezochromism, ionochromism, solvatochromism, and electrochromism [30].

Electrochromism is a phenomenon visibly reversible change in reflectance and/or transmittance under redox reactions. It is based on originating different absorption bands in the visible region along with switching between oxidation and reduction states. Generally, color change occurs between colored and transparent (bleached) states, or between two different color states. However, electrochromic materials can exhibit multiple color changes in case of existing available more than two redox states. This property is called poly-electrochromism or multicolor-electrochromism [31], [32].

Electrochromic materials -also called chromophores- can be classified into two main groups, which include inorganic materials such as transition metal oxides and alkali halides and organic materials, which include viologen and some conductive organic polymers.

Commonly used oxides of transition metals that are in the film form are manganese, cobalt, rhodium, ruthenium, iridium, and tungsten. They exhibit great electrochromic properties [30]. One of the most studied transition metal oxide as electrochromic material is tungsten trioxide (WO_3). Firstly, in the early 1800s, Berzelius stated that when pure WO_3, which is light yellow semi-conductor, was warmed by dry hydrogen gas, change in its color on reduction was monitored. After that, in 1824, Wöhler conducted the study in which is he monitored similar color change by chemical reduction of tungsten trioxide with sodium metal. However, in 1930, the first color change by electrochemical reduction of tungsten trioxide, which was coated on an

electrode in aqueous acid was reported in 1930 [33]. Basic color generation reaction of WO_3 thin film is:

$$WO_3 \text{ (transparent)} + x\ M^+ + x\ e^- \rightarrow M_xWO_3 \text{ (blue)}$$

Conjugated polymers as electrochromic materials attract much attention due to properties such as ease of visible absorption band tuning, conjugation length manipulating, implementing electron-donating and/or withdrawing groups, and controlling electronic and steric environment.

Owing to these properties, conjugated systems in their backbone of polymers have a great variety of electrochromic responses. Generally, conjugated polymers exhibit good electrochromic properties when they are in thin-film form. Redox switching results in new absorption bands of conjugated systems.

Polyaniline (PANI), also called aniline black, is one of the oldest investigated conjugated polymer which exhibits electrochromic properties. It has excellent features such as ease of process, low cost of production of conducting thin films that presents three specific color states to be called as one of the most appealing electrochromic conjugated polymer. Its polymer films have poly-electrochromic character which able to switch from insulating leucoemeraldine states (transparent) to conducting emeraldine state (yellow-green color) and lastly to pernigraniline state (blue-black color) [34].

There are four fundamental parameters that affect the efficiency of electrochromic materials, which include optical contrast, switching time, device stability, and optical memory.

1.5.1. Optical Contrast

Optical contrast is one of the most significant electrochromic factor to achieve high efficient electrochromic applications. Percent optical transmittance change ($\Delta T\%$) at a specific wavelength is called as optical contrast. This wavelength is specified by the value at which the highest absorption wavelength of the polymer film [35].

Throughout the redox reactions, degradation, which results in decreasing the optical contrast, is observed. This decrease in optical contrast leads to a reduction in the efficiency of electrochromic materials.

1.5.2. Switching Times

Another important parameter that plays an essential role in obtaining high efficient electrochromic applications is the switching time of materials. It is basically explained as the time needed to process from coloring to bleaching or from coloring to another coloring for electrochromic materials. Switching time increases when the electrochromic material is stable chemically. Factors that influence the switching time are the quantity of applied potential, the strength of ionic conductivity of electrolytes, transport ability of ions, and both thickness and morphology of the polymer films [36].

1.5.3. Device Stability

Device stability has a crucial impact on electrochromic device performance. It is explained as cyclic switching efficiency of electrochromic device without any degradation. There are several factors that affect the stability of electrochromic materials negatively, such as excess potential applied, side reactions as a result of moisture in the environment, and loss of heat, which can result from unstable resistance [37].

1.5.4. Optical Memory

Optical memory is defined as the period in which electrochromic devices can maintain a desired color. It plays a crucial role in order to determine the efficiency of electrochromic device performance. It can also be explained as the time it remains in the absorption state when the electric field is removed. Although optical memory could maintain for several days and/or weeks without any electrical current, for some EC devices replenishing of charges can be required to continue the charged state. The reason for this is that some undesirable reactions or short circuits could alter the desired color [38].

1.6. Organic Solar Cells

Currently, fossil fuels, which include coal, natural gases, and oil, are still dominating the worldwide energy supply. However, it is clear that awareness of the detrimental consequences of these non-renewable and contaminative energy sources have encouraged the search for renewable energy supplies. Solar energy without any exceptions is the renewable energy source that possesses the capability to address the world's enlarged and expanding energy needs. Solar cells at which sunlight is directly converted into electricity are one of the most promising, renewable, clean, and sustainable technologies compared with others [39].

Organic solar cells (OSCs) are devices that generate electricity from sunlight by using organic materials. Organic solar cells have considerable advantages over inorganic counterparts due to their distinctive features, which are flexible structure, lightweight, ability to be coated on plastic or glass substrates, easy to fabricate, and also low-cost production [40]. In addition to these, organic semiconductors possess high absorption coefficients, which facilitate to make highly thin films compared to inorganic materials. Therefore, these specific advantages of organic photovoltaic (OPV) devices make them great potential candidates for energy production [41].

The first generation of OPV devices was constructed using a single active layer, which was sandwiched between two electrodes. However, the power conversion efficiency (PCE) of these single-layer organic solar cells reached up to only 0.1%. Also, device performance of these solar cells was limited due to both low exciton dissociation and charge collection. In order to overcome these drawbacks, two new strategies were presented [42], [43]. The first one is bilayer organic solar cells, which have similar principles with p-n junction inorganic solar cells. Bilayer organic solar cell was firstly discovered by C. W. Tang with a power conversion efficiency of approximately 1%. However, these bilayer devices had several limitations, such as not efficient separation of excitons, high recombination of electron-hole process, and not efficient layer thickness to absorb sunlight. The second concept is designed as a blend of both donor

and acceptor materials spread throughout the active layer of a device. This concept is called bulk heterojunction (BHJ) solar cell, which is a more effective design to achieve high efficient OPV devices. For the last decades, bulk heterojunction solar cells have been gained more attention due to overcoming the limitation of efficient charge generation at the interface by utilizing a blend of donor-acceptor materials in the active layer [44], [45].

Although there are several advantages of OPV devices compared to inorganic counterparts, their short lifetimes and low power conversion efficiencies of organic solar cells limit their manufacturing on a large scale. Recently, enormous researches were developed to improve the lifetime, stability, and efficiency of OPV devices [46].

1.6.1. Device Architecture of Bulk Heterojunction OSCs

Bulk heterojunction type organic solar cell fundamentally consists of multilayered architecture. Each of these layers is constructed by a specific coating technique. Typical BHJ device architecture was depicted in Figure 1.9. Firstly, a transparent glass substrate is coated with transparent electron-conducting materials. Owing to excellent transparency and conductivity of indium tin oxide (ITO), it is utilized in BHJ device construction as an anode material. Then, the hole transport layer (HTL) is coated onto the ITO surface. Generally, a thin film of poly(3,4ethylene-dioxythiophene)-poly(styrenesulfonate) (PEDOT:PSS) is used as a hole transport layer in order to improve hole mobility and stability of BHJ solar cells. It also acts as an electron blocker towards any probable electron transfer from the acceptor unit due to possessing high LUMO energy level. The photoactive layer, which is comprised of a blend of donor and acceptor materials, is coated on the top of HTL. Commonly, conjugated polymers and organic small molecules are used as donor material, and fullerene derivatives are utilized as an acceptor material. Using donor-acceptor blend in active layer provides a reducing the exciton travel distance due to a large interface area between donor and acceptor materials. Therefore, charge separation is improved and could be achieved anywhere in the photoactive layer. The active layer is followed

by coating LiF as an electron transport layer (ETL) material and electrode with a low work function, respectively. There are several reasons that LiF is utilized with the cathode layer. The most important reason is that LiF provides a reduction in the active work function of cathode material; therefore, easier electron transportation occurs between LUMO of the acceptor and cathode layer. Also, thanks to its high boiling point nature, it protects the active layer from any degradation during the thermal deposition process of cathode material. Moreover, the LiF layer effectuates the smoother surface for cathode layer deposition, which results in enhancing contact standard between the active layer and the top electrode. Usually, calcium, aluminum or barium are utilized as the top electrode which is a cathode in order to collect the electrons generated in the photoactive layer [47]–[50].

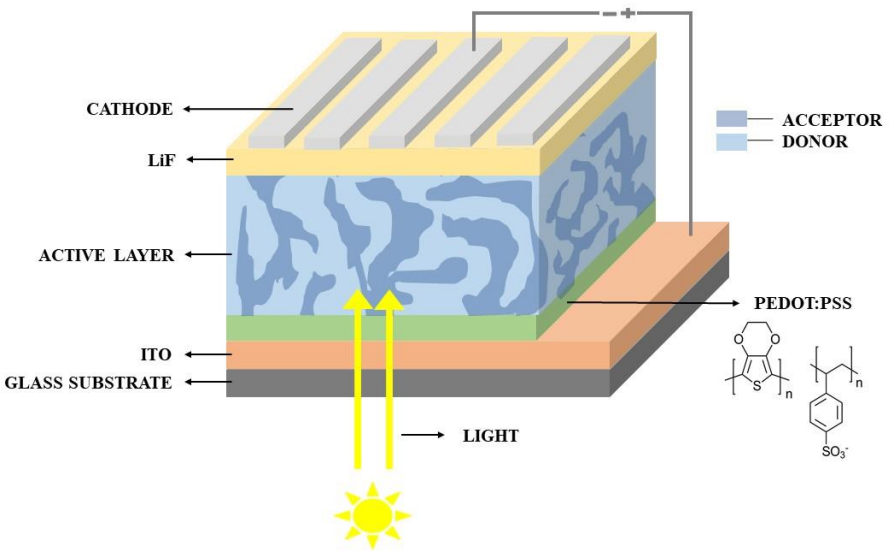

Figure 1.9. Schematic representation of bulk heterojunction organic solar cell device structure

1.6.2. Working Principles of OSCs

The fundamental working principle of the OSC device can be explained by four main steps, which are absorption of photons and formation of an exciton, exciton diffusion, dissociation of exciton, and charge transport and collection, respectively [48]. The schematic representation of the working principle of the OSC device was demonstrated in Figure 1.10. Firstly, the photon is absorbed by the illumination of photoactive material. Subsequently, the electrons are excited from the highest occupied molecular orbital (HOMO) to the lowest unoccupied molecular orbital (LUMO), while the positive charge carriers, which are also called holes, stay in the HOMO. Both negative and positive charge carriers are linked together and bounded by Coloumb forces. This attached charge carries form a Frankel exciton that is also named as electron-hole pair having binding energy between 0.1–1.4 eV. After the generation of excitons, they diffuse from the donor material to the interface of the donor and acceptor phases. Then, excitons which are at the donor-acceptor interface dissociate into both free electrons and holes. Frankel exciton binding energy is much higher than the excitons formed in the inorganic materials. In order to break this exciton binding energy and to achieve dissociation of an exciton without any recombination, both energy level offset of donor and acceptor material are utilized [46]. Due to the high exciton binding energy of organic materials, excitons could not dissociate at room temperature. Therefore, the extra driving force from acceptor material is required to achieve effective charge dissociation. Because of these, both donor and acceptor materials are used as blended forms in the active layer. Lastly, by the help of the internal electric field which results from electrodes with specific work functions, free charge carriers are separated and transferred to both donor and acceptor material. Charge carriers are collected at different electrodes. While electrons are collected at the cathode, holes are collected at the anode. Owing to all four fundamental steps which is completed the ideal circuit, the photo-current is generated successfully [27], [51]–[54].

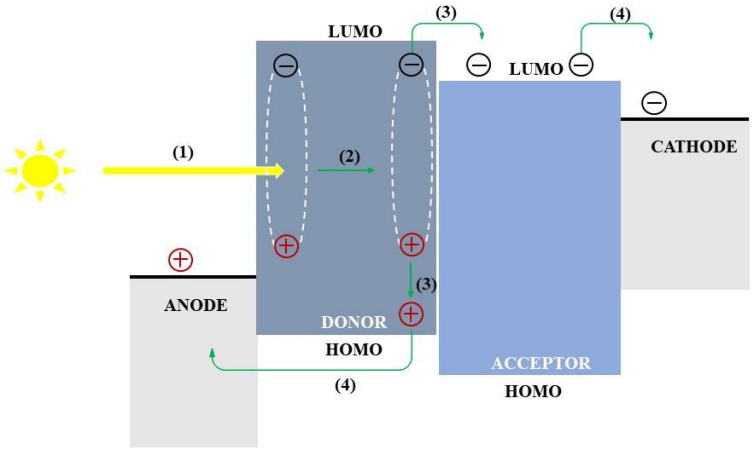

Figure 1.10. Schematic representation of the working principle of organic solar cells

1.6.3. Characterization of Organic Solar Cell Devices

In order to characterize the device performance of organic solar cells, the most significant determinant is the power conversion efficiency (PCE). The ratio between maximum output power (P_{max}) and incident light power (P_{in}) that is derived from current density-voltage characteristics under a standard air mass 1.5 global spectrum (AM1.5G) illumination conditions by using a solar simulator is termed as PCE of the organic solar cell device. AM 1.5 G is described as the sunlight radiation, which reaches the surface of the earth at an incident angle of 48^{o} for photovoltaic devices. Since AM 1.5 G is not the light intensity but the radiation spectrum, the power density of light is standardized at 100 mW/cm^2 for the photovoltaic application measurements [55]. The standard AM 1.5 G was illustrated in Figure 1.11.

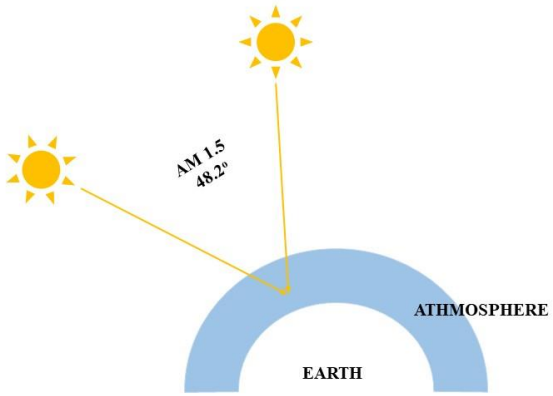

Figure 1.11. Illustration of AM 1.5 G Standardization

The PCE of the organic solar cell device is determined from the current density-voltage (J-V) curve, as demonstrated in Figure 1.12. With reference to the typical current density-voltage graph, solar cell measurements are performed under two different conditions, which are dark and illumination. However, the J-V curve passes through the origin due to appear almost no flow of current or potential under the dark condition measurements. The device generates power when it is performed under illumination, and the J-V curve presents in the fourth quadrant, which indicates the existing flow of current and potential [51], [56]. The photovoltaic power conversion efficiency (η_e) of the photovoltaic device is calculated from the given equation:

$$\eta e = \frac{Pmax}{Pin} = \frac{Voc * Jsc * FF}{Pin}$$

$$FF = \frac{Jmax * Vmax}{Jsc * Voc}$$

Where (P_{in}) is power of incident light, (P_{max}) is maximum power, (Voc) is open-circuit voltage, (Jsc) is short circuit current and, FF is the fill factor.

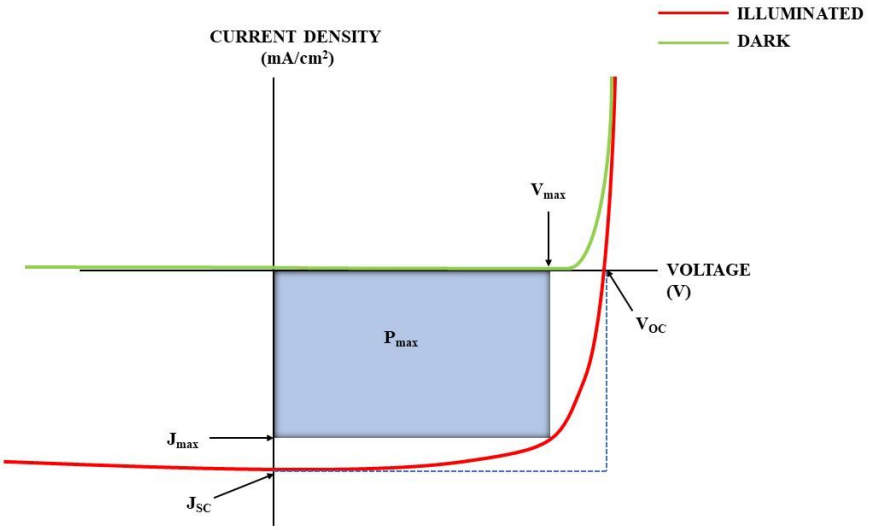

Figure 1.12. Typical current density-voltage characteristics of OPV device under illumination and dark

1.6.4. Substantial Parameters Influencing OSC Efficiency

1.6.4.1. Open Circuit Voltage

Open circuit voltage (V_{OC}) is described as the voltage output that is obtained from the circuit at zero current. It mainly depends on the current produced over radiation. In addition, in organic photovoltaic devices, V_{OC} directly depends on the highest occupied molecular orbital energy level of the donor molecule and lowest unoccupied molecular orbital energy level of the acceptor molecule. Therefore, the band gap of the donor-acceptor molecule has great effect on open-circuit voltage value [57].

Correlation between open circuit-voltage (V_{OC}) and energy levels of HOMO-LUMO is specified by the following equation:

$$Voc = \frac{1}{q}\left(E_{DONOR\ HOMO} - E_{ACCEPTOR\ LUMO}\right) - 0.3V$$

Where q is the elementary charge (q = 1.6 * 10^{-19} C), $E_{DONOR\ HOMO}$ is the magnitude of HOMO energy of the donor, and $E_{ACCEPTOR\ LUMO}$ is the magnitude of LUMO energy of the acceptor and 0.3V is the deviation value that is obtained from difference between theoretical maximum built-in potential (V_{BI}) and open circuit potential (V_{OC}). According to the following formula that gives the relationship between V_{OC} and HOMO-LUMO level of the molecule, open circuit voltage is linearly proportional to band gap alteration in donor-acceptor materials [58], [59].

1.6.4.2. Short Circuit Current Density

The term short circuit current density (J_{SC}) is described as a maximum current per unit area, which is generated by photovoltaic devices under illumination when there is no external voltage through the circuit. There is a direct relation between J_{SC} and the efficiency of solar cells because of light produced charge carriers. It bases upon several parameters such as cell area, the intensity of light, the incident light spectrum and also charge collection possibility of electrodes [60], [61].

Ideally, the short circuit current density J_{SC} is derived from the charge carrier density and charge carrier mobility in the organic semiconductor materials, which is specified by the following equation:

$$J_{SC} = nefIE$$

Where n is the charge carrier density, which is directly related to the band gap of the material, e is the elementary charge, fl is the charge carrier mobility, and E is the generated electric field. When a photovoltaic device with 100% efficiency is supposed, the term n is described as a number of absorbed atoms per unit area. The most critical factor in this equation is charge carrier mobility, which is the variable related to the device, not the material. It is profoundly affected by the nano-scale morphology of thin film that depends upon production techniques and conditions.

Nano-morphology could be altered by factors such as type of solvent, crystallization time of solvent, substrate temperature, or deposition techniques [62].

The electrical current generation of OSCs is evaluated by the number of collected charges at specific electrodes. It depends upon the qualifications of five steps, which occurred during the travel of charge carriers from an active layer to the specific electrodes. External quantum efficiency (EQE) is explained as bringing together all efficiencies of these steps [63]. Therefore, it is defined as the ratio between the number of incoming photons and the number of the generated charges. EQE can be derived from the following equation:

$$EQE = \eta_{abs} * \eta_{diff} * \eta_{diss} * \eta_{tr} * \eta_{cc}$$

Where η_{abs} is the absorption efficiency of photovoltaic device, η_{diff} is the exciton capability to diffuse into the donor-acceptor interface, η_{diss} is the dissociation efficiency of excitons, η_{tr} is the efficiency of charge transfer process of device and η_{cc} is the charge collection efficiency of the device.

1.6.4.3. Fill Factor

Fill factor (FF) is one of the most essential determinants that directly influences the power conversion efficiency of OSCs. It is described as the ratio of maximum power (P_{max}) generated from the photovoltaic device to the product of the short circuit current density (J_{SC}) and the open-circuit voltage (V_{OC}) [63]. It is formulized by the following equation:

$$FF = \frac{Jmax * Vmax}{Jsc * Voc}$$

The fill factor (FF) is correlated to two primary components of the photovoltaic device circuit, which are named as series resistance (R_s) and shunt resistance (R_{sh}) of device.

For the ideal situation, the maximum power (P_{max}) generated by the device under illumination is equal to the multiplication of J_{SC} and V_{OC}; therefore, the J-V curve of OPV device is rectangular. However, in practice, maximum power is confined with the product of J_{max} and V_{max} due to both existing recombination at the donor-acceptor interface and deviation of the diode from an ideal case. In an an ideal case for diode, series resistance should be zero, whereas shunt resistance goes to infinity. Shunt resistance (R_{sh}) is basically described as a parameter that is associated with charge carriers recombination at close donor-acceptor interface [64]. It can be evaluated by taking inverse slope from J-V graph of device at 0 V. Decreasing in R_{sh} causes to different current pathway that leads to a decrease in the flow of current through the OPV device. Moreover, series resistance (R_s) is described as a parameter that is related to the mobility of charge carriers. The existence of traps in the device system reduces the charge carriers which results in enhancing the travel distance of these charge carriers. This enhancement leads to an increase in series resistance. It can be estimated by taking slope from the J-V graph of device where V_{OC} at a positive quadrant [46].

1.7. Literature Studies of Benzodithiophene Containing Polymer Solar Cells

Benzodithiophene (BDT) is one of the most promising electron-rich donor moieties for conjugated polymers to achieve high power conversion efficiency photovoltaic applications. Due to its highly planar and fused structural characteristics, the BDT unit provides enhancing the electron delocalization, and therefore, charge carrier mobility increases exceedingly. Moreover, its 2D conjugated structure provides both strong inter-chain features and wide light absorption owing to its broaden side chain [65]. Furthermore, introducing the side chains such as alkyl, alkoxy or aryl groups to the benzodithiophene unit can be easily achieved. These attached groups provide not only increasing the solubility of the corresponding polymers but also enhancing the π-conjugation length from the backbone to the attached group. Therefore, while band gap of the corresponding polymer decreases, the charge carrier mobilities increase. BDT based polymers for organic solar cell applications have been observed to demonstrate considerably enhanced power conversion efficiencies. In addition,

introducing the alkyl-selenophene unit to the BDT moiety has demonstrated high power conversion efficiency for organic solar cells. Because of strong intermolecular Se-Se interactions, selenophene based BDT moiety provides enhancing conductivity. Moreover, due to having a bigger size of selenium and a more polarizable feature than sulfur, hole mobility increases in selenium containing polymers in compare to thiophene analogs [20]. In literature, several studies have shown that BDT based copolymers coupled with suitable acceptors in terms of energy levels and absorption properties have high potential to achieve high performance organic solar cells. In 2017, Hyeongjin Hwang et al. reported that 4,8-bis(5-(2-ethylhexyl)selenophen-2-yl)benzo[1,2-b:4, 5-b']dithiophene and 5-(undecan-5-yl)-4H-thieno[3,4-c]pyrrole-4,6 (5H)-dione based π-conjugated polymer utilized with 3-octylthieno[3,2-b]thiophene as π-bridge moiety (PBT-ODT) (Figure 1.13) reached 7.21% PCE in BHJ organic solar cell application. V_{OC}, J_{SC}, and FF of the organic BHJ solar cell were measured as 0.87 V, 12.19 mA/cm^2 and 68% respectively by utilizing polymers/$PC_{71}BM$ blends (1:1.5, w/w) [66]. In addition, Samuel C. Price et. al synthesized 4,8-bis(3-pentyloctyl)benzo[1,2-b:4,5-b']di- thiophene and 5,6-difluoro-2-(undecan-5-yl)-2H-benzo[d][1,2,3]triazole comprising polymer with thiophene π-bridge unit PBnDT-FTAZ (Figure 1.13) with 6.03% PCE in 2011 [67]. Furthermore, In 2011, Jian-Ming Jianget al. reported that 4,8-bis(2-ethylhexyl)benzo[1,2-b:4,5-b']dithiophene and 5,6-bis(octyloxy)benzo[c][1,2,5]oxa- diazole containing copolymer with utilized thiophene as π-bridge moiety PBDTBO (Figure 1.13) showed 5.7% PCE and V_{OC}, J_{SC}, and FF of the organic BHJ solar cell were measured as 0.86 V, 10.4 mA/cm^2 and 64.4% respectively by using polymers/$PC_{61}BM$ blends (1:1, w/w) [68].

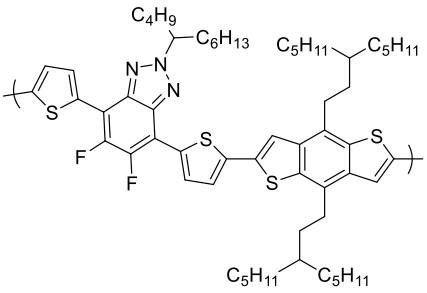

PBnDT-FTAZ

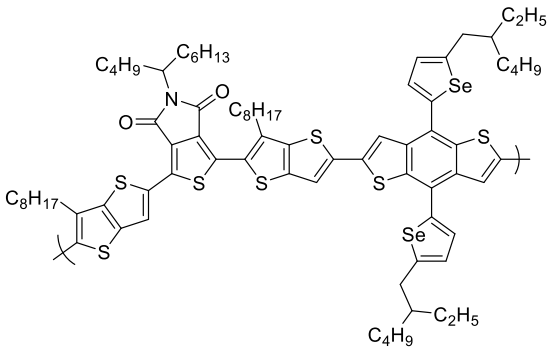

PBT-ODT

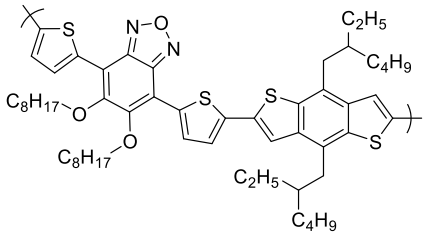

PBDTBO

Figure 1.13. Molecular structures of BDT based PBnDT-FTAZ, PBT-ODT and PBDTBO

1.8. Aim of the Thesis Study

The aim of the study is to design and synthesize novel donor-acceptor type alternating conjugated polymers for organic photovoltaic applications. The donor-acceptor (D-A) approach is the primarily utilized technique to design π-conjugated copolymers, which have a narrow band gap. Copolymers, which is designed by applying the donor-acceptor approach, basically includes repetitive alternating donor (D) and acceptor (A) moieties in their main chains. For this purpose, two donor-acceptor type alternating polymers that have benzotriazole based acceptor moiety and benzodithiophene based donor moiety with different π-bridge groups were synthesized via Stille coupling reaction to realize the impacts of structural modifications on electrochemical and

optoelectronic properties. While P1 has thiophene π-bridge, P2 has selenophene π-bridge in their backbones. After desired polymers were successfully synthesized, their optical, electrochemical, and device characterizations were studied. The effects of utilizing different π-bridge units in polymer backbones on properties of polymers were examined. The molecular structure of desired synthesized polymer P1 was shown in Figure 1.14, and polymer P2 was illustrated in Figure 1.15.

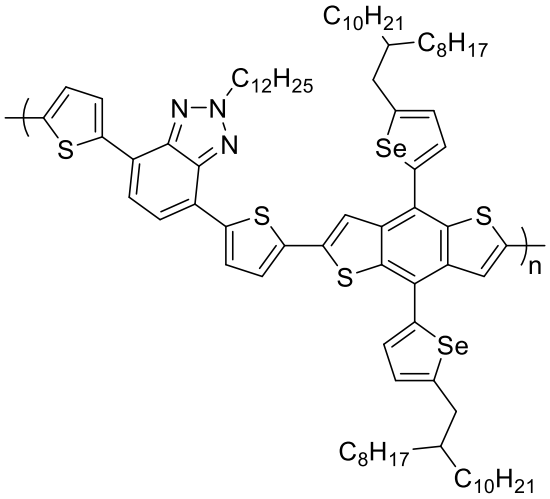

Figure 1.14. Molecular structure of **P1**

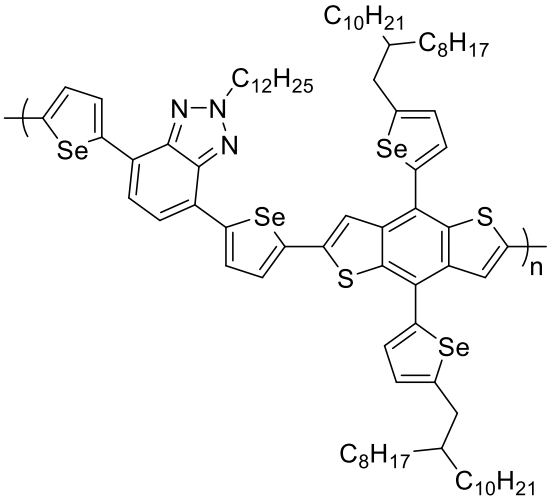

Figure 1.15. Molecular structure of **P2**

CHAPTER 2

EXPERIMENTAL

2.1. Materials and Equipment

All chemicals used in the synthesis of both monomers and polymers were provided from Sigma Aldrich Chemical Co. Ltd. $PC_{71}BM$ used as acceptor moiety in organic solar cell device was purchased from Sollene. Toluene and tetrahydrofuran (THF) were dried by using benzophenone and metallic sodium and were used in the reaction freshly. Other solvents required for the reactions were used without further purification procedures. Reactions that were sensitive to air and moisture were performed under the nitrogen atmosphere. In order to purify the crude materials, the column chromatography technique was performed by using Merc Silica Gel 60 as the stationary phase with different solvent systems.

In order to determine and prove chemical structures of synthesized materials, Nuclear Magnetic Resonance Spectroscopy technique was used. Both ^{1}H and ^{13}C NMR spectra of materials were examined in deuterated chloroform ($CDCl_3$). They were performed via Bruker Spectrospin Avance DPX-400 model Spectrometer with regard to trimethylsilane (TMS) as the internal reference.

Gel permeation chromatography (GPC) technique in which polystyrene is taken as a standard reference was utilized to determine the average molecular weights of the polymers in chloroform ($CDCl_3$). Varian Cary 5000 model UV-Vis Spectrometer was employed to accomplish spectrochemical studies of synthesized polymers at ambient temperature. Gamry 600 potentiostat was used to achieve cyclic voltammetry studies of polymers.

For investigating the thermal features of synthesized polymers, thermogravimetry analysis (TGA) and diffential scanning calorimetry (DSC) were performed.

2.2. Synthesis of Monomers

2.2.1. Synthesis of 4,7-dibromobenzo[c][1,2,5]thiadiazole

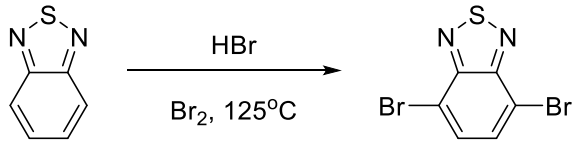

Figure 2.1. Synthesis of 4,7-dibromobenzo[c][1,2,5]thiadiazole

Benzo-1,2,5-thiadiazole (6.00 g, 44.06 mmol) and 70 mL HBr were put into a three necked round bottom reaction flask and were allowed to be dissolved at room temperature. After obtaining well dissolved mixture, reaction temperature was raised to 95 ^{o}C and the reaction mixture was stirred for one hour at this temperature. After one hour, bromine solution (21.12 g, 132.19 mmol) in 25 mL HBr was added to reaction mixture drop by drop, and the reaction mixture was allowed to reflux overnight at 130 ^{o}C. After the mixture was cooled to room temperature, 400 mL saturated sodium bisulfate solution ($NaHSO_3$) was added into the reaction flask to consume excess bromine completely. Then, the residue was percolated by filter paper and sluieced with distilled water and diethyl ether, repeatedly. Collected pale yellow solid dried under vacuum to afford 4,7-dibromobenzo[c][1,2,5]thiadiazole (11.30 g, 87.2%).

2.2.2. Synthesis of 3,6-dibromocyclohexa-3,5-diene-1,2-diamine

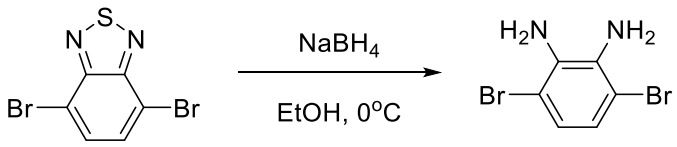

Figure 2.2. Synthesis of 3,6-dibromocyclohexa-3,5-diene-1,2-diamine

4,7-Dibromobenzo[c][1,2,5]thiadiazole (11.00 g, 37.42 mmol) was put into a 1 L round bottom reaction flask containing 300 mL of ethanol at 0 °C. After that, $NaBH_4$ (28.31 g, 748.39 mmol) powder was added portion-wise into the reaction mixture carefully and then it was allowed to be stirred at 0 °C for 40 min. After 40 min, the mixture was allowed to reach room temperature and stirred overnight. Then, ethanol was eliminated under reduced pressure, and the resulting reaction medium was washed with brine and diethyl ether several times. Then, the organic phase was dried over $MgSO_4$, and the solvent was removed under reduced pressure to afford the 3,6-dibromocyclohexa-3,5-diene-1,2-diamine as the final product (6.8 g, 67.8%).

2.2.3. Synthesis of 4,7-dibromo-2H-benzo[d][1,2,3]triazole

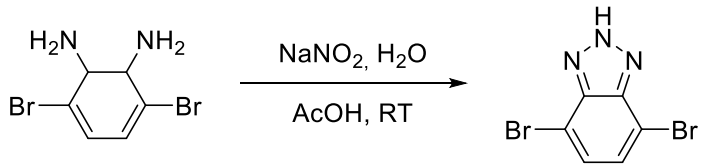

Figure 2.3. Synthesis of 4,7-dibromo-2H-benzo[d][1,2,3]triazole

3,6-Dibromocyclohexa-3,5-diene-1,2-diamine (6.50 g, 24.26 mmol) was put into a round-bottom reaction flask containing 75 mL of glacial acetic acid. Then, sodium nitrate (1.84 g, 26.68 mmol) solution in 25 mL H_2O was added drop by drop into the reaction mixture and allowed to be stirred for 3 hours at room temperature. After 3 hours of stirring, the precipitate was filtered under vacuum and washed with water several times. The crude product was dried to obtain 4,7-dibromo-2H-benzo[d][1,2,3]triazole as the final product (3.90 g, 58.1%).

2.2.4. Synthesis of 4,7-dibromo-2-dodecyl-2H-benzo[d][1,2,3]triazole

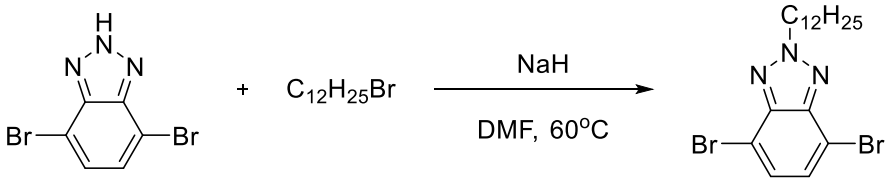

Figure 2.4. Synthesis of 4,7-dibromo-2-dodecyl-2H-benzo[d][1,2,3]triazole

4,7-Dibromo-2H-benzo[d][1,2,3]triazole (3.50 g, 12.64 mmol) was put into a two necked rounded reaction flask under nitrogen atmosphere. After that, 12 mL of dimethyl formamide (DMF) was added by syringe to dissolve the 4,7-dibromo-2H-benzo[d][1,2,3]triazole in the reaction flask. Then, NaH (0.36 g, 15.17 mmol) was added to the reaction mixture at 0 ºC in the ice bath. After the insertion of NaH was performed, the reaction temperature was risen to 70 ºC, following by addition of 1-bromododecane (3.78 g, 15.17 mmol) into the reaction mixture. Reaction was allowed to be stirred at 70 ºC overnight. Then, the reaction mixture and 300 mL of water were put into the 1000 mL of extraction funnel to be extracted with chloroform repeatedly. The resulting organic layer was clarified with water four times and dried over anhydrous $MgSO_4$. The solvent was removed under reduced pressure. Further purification was achieved by silica gel column chromatography with chloroform and hexane (2:1) to afford 4,7-dibromo-2-dodecyl-2H-benzo[d][1,2,3]triazole as dark yellow (2.70 g, 48%).

^{1}H NMR (400 MHz, $CDCl_3$) δ 7.44 (s, 2H), 4.77 (t, *J* = 7.4 Hz, 2H), 2.18 – 2.10 (m, 2H), 1.36 – 1.21 (m, 18H), 0.87 (t, *J* = 6.7 Hz, 3H). **^{13}C NMR** (101 MHz, CDCl3) δ 143.72, 129.51, 109.98, 57.49, 31.90, 30.22, 29.57, 29.59, 29.48, 29.36, 29.34, 28.98, 26.50, 22.68, 14.12.

2.2.5. Synthesis of tributyl(thiophen-2-yl)stannane

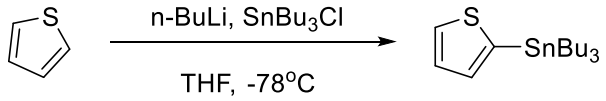

Figure 2.5. Synthesis of tributyl(thiophen-2-yl)stannane

The solution of *n*-butyl lithium (2.40 g, 2.5 M in hexane, 37.44 mmol) was added drop by drop into the reaction solution of thiophene (3.00 g, 35.66 mmol) dissolved in freshly distilled THF (30 mL) in two necked rounded reaction flask under an nitrogen atmosphere at -78 ^{o}C . Then, the reaction mixture was allowed to be stirred for one hour at -78 ^{o}C. After that, tributyltin chloride (13.93 g, 42.79 mmol) was added slowly within 20 minutes, following by stirring for another 1 hour at -78 ^{o}C. Then, the reaction mixture was allowed to reach to room temperature and stirred overnight. Next, the solvent was eliminated from reaction mixture under reduced pressure, and then, the resulting reaction medium was poured into the 500 mL of extraction funnel. Extration of reaction medium presented in water was performed with dichloro methane several times. Then, the organic phase was sluiced with brine and saturated NH_4Cl solution three times and dried over anhydrous $MgSO_4$. Thereafter evaporation of solvent, a brownish- yellow liquid was obtained (11.50 g, 86%).

2.2.6. Synthesis of 2-dodecyl-4,7-di(thiophen-2-yl)-2H-benzo[d][1,2,3]triazole

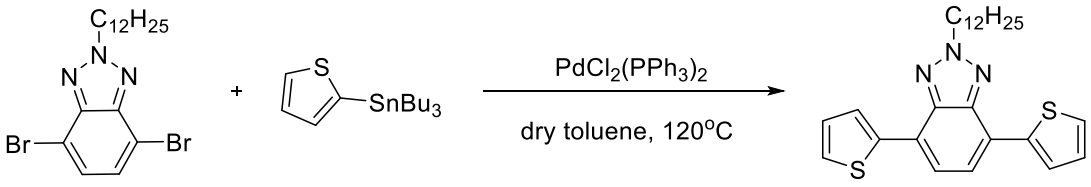

Figure 2.6. Synthesis of 2-dodecyl-4,7-di(thiophen-2-yl)-2H-benzo[d][1,2,3]triazole

4,7-Dibromo-2-dodecyl-2H-benzo[d][1,2,3]triazole (0.30 g, 0.67 mmol) and tributyl-(thiophen-2-yl)stannane (0.75 g, 2.02 mmol) were put into a two necked rounded flask under nitrogen atmosphere. Subsequently, dry toluene (25 mL) was added by syringe into the reaction flask to dissolve the reactants. The reaction mixture was purged with nitrogen for 1 hour, following by $PdCl_2(PPh_3)_2$ (108.78 mg, 0.15 mmol) was added. Then, reaction mixture was refluxed at 120 ^oC under nitrogen atmosphere overnight. The solvent removal process was performed via reducing pressure. For purification of residual product, silical gel column chromatography was performed with hexane and chloroform (3 Hexane :1 $CHCl_3$) solvent system. 2-dodecyl-4,7-di(thiophen-2-yl)-2H-benzo[d] [1,2,3]triazole (greenish-yellow solid) was obtained as a final product. (0.25 g, 82%)

^{1}H NMR (400 MHz, $CDCl_3$) δ 8.10 (d, J = 2.6 Hz, 2H), 7.63 (s, 2H), 7.38 (d, J = 4.0 Hz, 2H), 7.19 (dd, J = 5.1, 3.7 Hz, 2H), 4.82 (t, J = 7.3 Hz, 2H), 2.24 – 2.16 (m, 2H), 1.40 – 1.20 (m, 18H), 0.87 (t, J = 6.8 Hz, 3H). **^{13}C NMR** (101 MHz, CDCl3) δ 142.10, 139.98, 128,10, 126,97, 125.53, 123.60, 122.77, 56.88, 31.91, 30.08, 29.62, 29.63, 29.56, 29.44, 29.34, 29.05, 26.61, 22.69, 14.12.

2.2.7. Synthesis of 4,7-bis(5-bromothiophen-2-yl)-2-dodecyl-2H-benzo[d][1,2,3] triazole

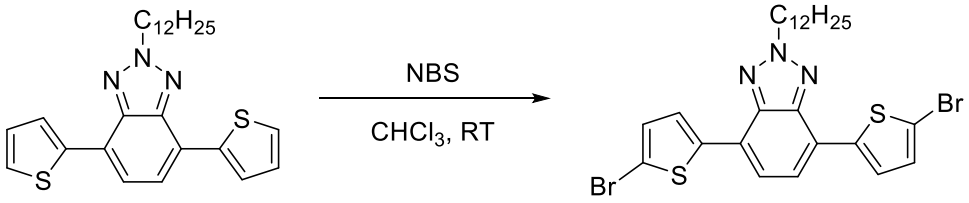

Figure 2.7. Synthesis of 4,7-bis(5-bromothiophen-2-yl)-2-dodecyl-2H-benzo[d][1,2,3] triazole

Under dark, the compound of 2-dodecyl-4,7-di(thiophen-2-yl)-2H-benzo[d][1,2,3] triazole (0.22 g, 0.49 mmol) and in $CHCl_3$ (25 mL) were put into the one necked round

reaction flask at room temperature. After dissolving of 2-dodecyl-4,7-di(thiophen-2-yl)-2H-benzo[d][1,2,3]triazole in chloroform solvent completed, N-bromosuccinimide (NBS) (0.17 g, 0.97 mmol) was added in small portions into the reaction solution. After the addition of NBS was finished, the reaction mixture was allowed to be stirred overnight in the dark, following by washing with saturated $NaHCO_3$, and brine several times and drying over $MgSO_4$. Then, the solvent was evaporated under reduced pressure. No need any further purifications to afford 4,7-bis(5-bromothiophen-2-yl)-2-dodecyl-2H-benzo[d][1,2,3] triazole as a yellow solid (0.29 mg, 97%).

^{1}H NMR (400 MHz, $CDCl_3$) δ 7.78 (d, *J* = 3.9 Hz, 2H), 7.49 (s, 2H), 7.12 (d, *J* = 3.9 Hz, 2H), 4.79 (t, *J* = 7.2 Hz, 2H), 2.22 – 2.13 (m, 2H), 1.42 – 1.22 (m, 18H), 0.87 (t, *J* = 6.8 Hz, 3H). **^{13}C NMR** (101 MHz, CDCl3) δ 141.72, 141.24, 130.89, 126.95, 123.00, 122.20, 113.17, 56.94, 31.92, 30.04, 29.63, 29.55, 29.57, 29.44, 29.35, 29.02, 26.57, 22.70, 14.13.

2.2.8. Synthesis of tributyl(selenophen-2-yl)stannane

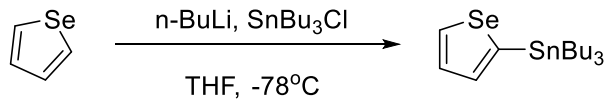

Figure 2.8. Synthesis of tributyl(selenophen-2-yl)stannane

A solution of selenophene (1.50 g, 11.45 mmol) in freshly distilled THF (20 mL) in two necked rounded reaction flask under nitrogen atmosphere was stirred until reaction temprature reached to -78 °C . Then, *n*-butyl lithium solution (0.77 g, 2.5 M in hexane, 12.02 mmol) was added drop wise very slowly into the mixture at -78 °C, following by stirring the reaction mixture for more 1 hour at this temperature. After that, addition of tributyltin chloride (4.47 g, 13.74 mmol) was performed slowly within 15 minutes, following by stirring the reaction mixture for another 1 hour at -78 °C.

Then, the reaction mixture was allowed to reach to the room temperature and was stirred overnight. The mixture was put in solvent removal process under reduced pressure and then, residual product was extracted with water and dichloromethane several times. The organic phase was sluiced with brine and sufficient amount of saturated NH_4Cl and dried over $MgSO_4$, respectively. After the removal of the solvent process, a dark yellow liquid was obtained as a final product (3.70 g, 76%).

2.2.9. Synthesis of 2-dodecyl-4,7-di(selenophen-2-yl)-2H-benzo[d][1,2,3]triazole

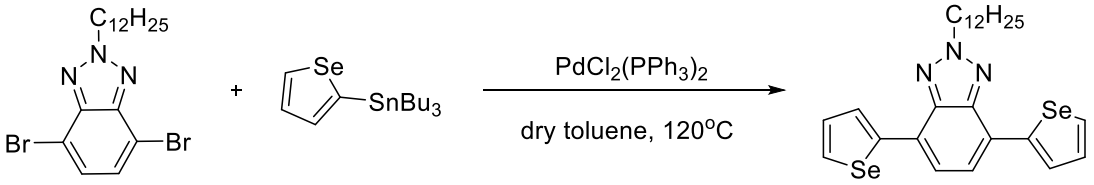

Figure 2.9. Synthesis of 2-dodecyl-4,7-di(selenophen-2-yl)-2H-benzo[d][1,2,3]triazole

A solution of 4,7-dibromo-2-dodecyl-2H-benzo[d][1,2,3]triazole (0.20 g, 0.45 mmol) and tributyl(thiophen-2-yl)stannane (0.57 g, 1.35 mmol) in dry toluene (20 mL) was stirred under nitrogen atmosphere. After that, the reaction solution was purged with nitrogen for more 1 hour, followed by addition of $PdCl_2(PPh_3)_2$ (72.52 mg, 0.10 mmol). Then, the reaction mixture was put in reflux process overnight at 120 ^oC. The solvent removing process was achieved under reduced pressure. For purification of residual product, silica gel column chromatography was carried out with hexane and dichloromathane (2:1) solvent system to afford 2-dodecyl-4,7-di(selenophen-2-yl)-2H -benzo[d][1,2,3]triazole as a yellow solid (0.18 g, 71%)

^{1}H NMR (400 MHz, CDCl3) δ 8.20 (d, J = 3.0 Hz, 2H), 8.08 (d, J = 4.7 Hz, 2H), 7.60 (s, 2H), 7.42 (dd, J = 5.6, 3.9 Hz, 2H), 4.82 (t, J = 7.2 Hz, 2H), 2.24 – 2.16 (m, 2H), 1.32 – 1.20 (m, 18H), 0.87 (t, J = 6.8 Hz, 3H). **^{13}C NMR** (101 MHz, CDCl3) δ 145.18,

141.92, 131.42, 130.49, 128.21, 125.46, 123.02, 56.85, 31.93, 29.99, 29.64, 29.58, 29.56, 29.46, 29.36, 29.06, 26.61, 22.70, 14.14.

2.2.10. Synthesis of 4,7-bis(5-bromoselenophen-2-yl)-2-dodecyl-2Hbenzo[d] [1,2,3]triazole

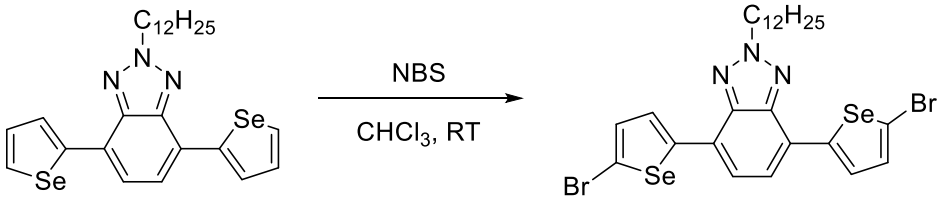

Figure 2.10. Synthesis of 4,7-bis(5-bromoselenophen-2-yl)-2-dodecyl-2H-benzo[d][1,2,3]triazole

Under dark, 2-dodecyl-4,7-di(selenophen-2-yl)-2H-benzo[d][1,2,3]tri-azole (0.16 g, 0.29 mmol) in $CHCl_3$ (20 mL) was stirred for 15 min at room temperature. After 15 min stirring, N-bromosuccinimide (NBS) (0.11 g, 0.59 mmol) was slowly added in small portions over 45 min. After the total addition of N-bromosuccinimide, the reaction mixture was allowed to stirred overnight at room temperature in the dark environment. The reaction medium was sluiced with sufficient amount of saturated $NaHCO_3$ and brine several times, and was exsiccated over $MgSO_4$, respectively. Then, the solvent removing process was achieved by reduced pressure. To purify the residual product, silica gel column chromatography was carried out with hexane and ethyl acetate (5:1) solvent system to afford 4,7-bis(5-bromoselenophen-2-yl)-2-dodecyl-2H-benzo[d][1,2,3]triazole as a brownish-yellow solid (0.19 mg, 92%).

^{1}H NMR (400 MHz, $CDCl_3$) δ 7.79 (d, J = 4.2 Hz, 2H), 7.52 (s, 2H), 7.33 (d, J = 4.2 Hz, 2H), 4.79 (t, J = 7.1 Hz, 2H), 2.22 – 2.14 (m, 2H), 1.40 – 1.19 (m, 18H), 0.87 (t, J = 6.8 Hz, 3H). **^{13}C NMR** (101 MHz, CDCl3) δ 146.46, 141.65, 133.64, 127.27, 124.82, 121.84, 117.63, 56.93, 31.92, 29.92, 29.66, 29.64, 29.57, 29.46, 29.35, 29.00, 26.56, 22.70, 14.13.

2.2.11. Synthesis of 2-(2-octyldodecyl)selenophene

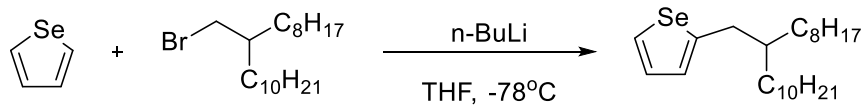

Figure 2.11. Synthesis of 2-(2-octyldodecyl)selenophene

A solution of selenophene (1.20 g, 9.16 mmol) in freshly distilled THF (20 mL) was stirred under nitrogen atmosphere until the reaction temperature reached to -78 °C. Thereafter, *n*-butyl lithium solution (0.65 g, 2.5 M in hexane, 10.07 mmol) was slowly added dropwise into the reaction mixture at the same temperature. After the total addition of *n*-butyl lithium completed, the reaction mixture was allowed to be stirred for another 30 minutes at -78 °C and then 1 hour at room temperature, respectively. It was followed by the addition of 9-(bromomethyl)nonadecane (3.64 g, 10.07 mmol) in one portion at -78 °C. Then, the reaction mixture was allowed to be refluxed overnight at 85 °C. The reaction medium was quenched excessively with water and then, extracted with dichloro methane several times. The resulting organic phase was sluiced with brine and water, respectively and was exsiccated over $MgSO_4$. Then, the solvent was put in removal process under reduced pressure. To purify the residual product, silica gel column chromatography was carried out with hexane to afford 2-(2-octyldodecyl)selenophene as light yellow oil (2.10 g, 55%).

^{1}H NMR (400 MHz, $CDCl_3$) δ 7.81 (d, J = 4.6 Hz, 1H), 7.13 (dd, J = 5.6, 3.6 Hz, 1H), 6.92 (d, J = 2.7 Hz, 1H), 2.83 (d, J = 6.5 Hz, 2H), 1.64 – 1.51 (m, 1H), 1.44 – 1.16 (m, 32H), 0.90 (t, J = 6.7 Hz, 6H). **^{13}C NMR** (101 MHz, $CDCl_3$) δ 151.98, 128.97, 128.19, 127.29, 40.83, 36.92, 33.95, 33.16, 31.96, 31.61, 30.81, 29.99, 29.88, 29.69 29.59, 29.39, 29.37, 26.77, 26.62, 22.73, 14.15.

2.2.12. Synthesis of 4,8-bis(5-(2-octyldodecyl)selenophen-2-yl)benzo[1,2-b:4,5-b'] dithiophene

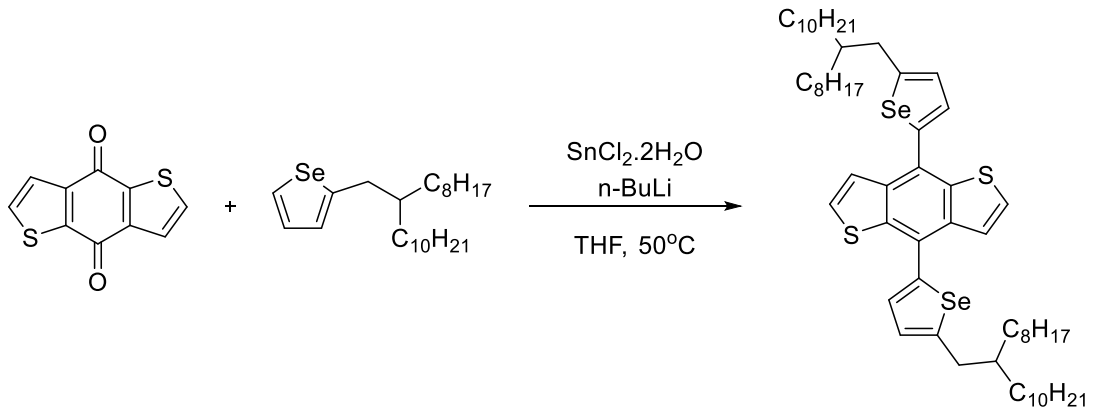

Figure 2.12. Synthesis of 4,8-bis(5-(2-octyldodecyl)selenophen-2-yl)benzo[1,2-b:4,5-b']dithiophene

The solution of 2-(2-octyldodecyl)selenophene (1.12 g, 2.72 mmol) in dry THF (40 mL) in two necked rounded reaction flask was stirred under nitrogen atmosphere until the reaction temperature reached to 0 ^{o}C in ice bath. Thereafter, drop wise addition of *n*-butyl lithium solution (0.23 g, 2.5 M in hexane, 3.63 mmol) was performed into the reaction mixture at 0 ^{o}C. After the entire addition of *n*-butyl lithium, the reaction mixture was allowed to be heated to 50 ^{o}C, and was stirred for 2 hours at the same temperature. Then, benzo[1,2-b:4,5-b']dithiophene-4,8-dione (0.20 g, 0.91 mmol) was added to the reaction mixture in one portion and stirred at 50 ^{o}C for another 2 hours. After that, the reaction mixture was cooled to room temperature, and tin (II) chloride dihydrate (1.70 g, 7.54 mmol) in 15% HCl (10 mL) was added. Thereafter, the reaction mixture was allowed to be stirred for another 3 hours at the same temperature. After the reaction was completed entirely, the reaction medium was taken into ice-water. It was followed by the extraction with diethyl ether several times. The resulting organic phase was sluiced with brine and water, respectively and was exsiccated over anhydrous $MgSO_4$. Then, removal of solvent process was achieved under reduced

pressure. For purification of residual product, silica gel column chromatography was carried out with only hexane solvent system to obtain 4,8-bis(5-(2-octyldodecyl) selenophen-2-yl)benzo[1,2-b:4,5-b']dithiophene as sticky brownish-yellow viscous oil (0.55 g, 60%).

^{1}H NMR (400 MHz, $CDCl_3$) δ 7.66 (d, *J* = 5.7 Hz, 2H), 7.44 (d, *J* = 5.6 Hz, 2H), 7.40 (d, *J* = 3.6 Hz, 2H), 7.03 (d, *J* = 3.6 Hz, 2H), 2.91 (d, *J* = 6.5 Hz, 4H), 1.73 – 1.66 (m, 2H), 1.41 – 1.24 (m, 64H), 0.91 – 0.86 (m, 12H). **^{13}C NMR** (101 MHz, $CDCl_3$) δ 153.89, 142.77, 138.81, 136.24, 130.02, 127.54, 127.39, 126.28, 123.53, 40.81, 37.44, 33.36, 31.97, 30.02, 29.71, 29.68, 29.41, 26.69, 22.73, 14.16.

2.2.13. Synthesis of (4,8-bis(5-(2-octyldodecyl)selenophen-2-yl)benzo[1,2-b:4,5-b']dithiophene-2,6-diyl)bis(trimethylstannane)

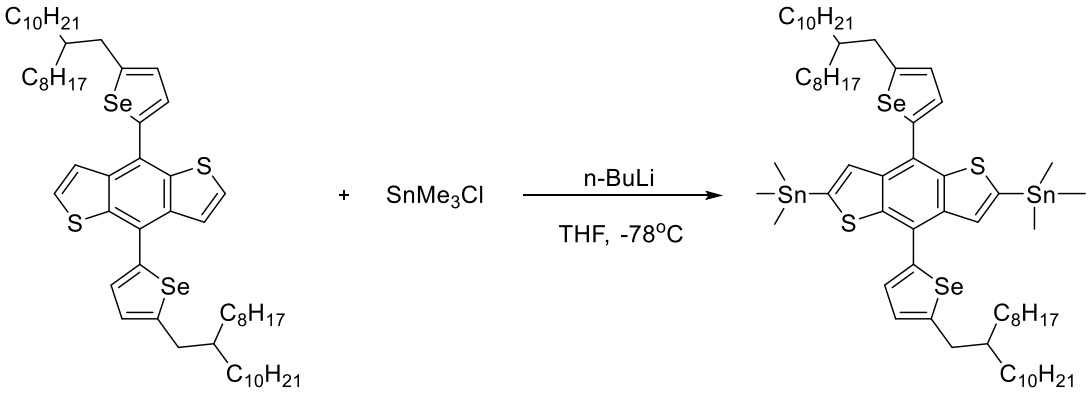

Figure 2.13. Synthesis of (4,8-bis(5-(2-octyldodecyl)selenophen-2-yl)benzo[1,2-b:4,5-b']dithiophene-2,6-diyl)bis(trimethylstannane)

The solution of 4,8-bis(5-(2-octyldodecyl)selenophen-2-yl)benzo[1,2-b:4,5-b']dithiophene (0.46 g, 0.46 mmol) in dry THF (25 mL) placed in a three necked rounded reaction flask was stirred under nitrogen until the reaction mixture reached to -78 °C via dry-ice/acetone. Thereafter, *n*-butyl lithium solution (0.23 g, 2.5 M in hexane, 3.63 mmol) was added gradually into the reaction mixture. It was followed by stirring of

reaction mixture for 15 min at -78 ^{o}C. Then, trimethyltin chloride solution (0.29 g, 1 M in THF, 1.46 mmol) was added to the reaction mixture in one portion at the same temperature. After that, the mixture was allowed to reach to room temperature and was stirred overnight at that temperature. The reaction mixture was taken into ice-water, subsequently and then, the resulting mixture was extracted with diethyl ether. After entire extraction process, the resulting organic phase sluiced with brine repeatedly and exsiccated over anhydrous $MgSO_4$. Then, the evaporation of solvent process was achieved under reduced pressure. There was no need for any further purification to afford (4,8-bis(5-(2-octyldodecyl) selenophen-2-yl)benzo[1,2-b:4,5-b']dithiophene-2,6-diyl)bis(trimet- hyl stannane) as sticky dark yellow viscous oil (0.48 g, 78%).

^{1}H NMR (400 MHz, $CDCl_3$) δ 7.74 (s, *J* = 14.8 Hz, 2H), 7.46 (d, *J* = 3.6 Hz, 2H), 7.07 (d, *J* = 3.6 Hz, 2H), 2.95 (d, *J* = 6.5 Hz, 4H), 1.82 – 1.69 (m, 2H), 1.35 – 1.28 (m, 64H), 0.85 – 0.80 (m, 12H), 0.50 – 0.37 (m, 18H). **^{13}C NMR** (101 MHz, $CDCl_3$) δ 153.51, 143.66, 142.19, 138.94, 137.06, 131.35, 129.82, 127.50, 124.63, 40.77, 37.49, 33.45, 31.97, 30.07, 29.74, 29.41, 29.31, 29.19, 27.45, 27.29, 26.76, 22.74, 14.15, 13.75, 9.49, 8.77.

2.3. Synthesis of Polymers

2.3.1. Synthesis of P1

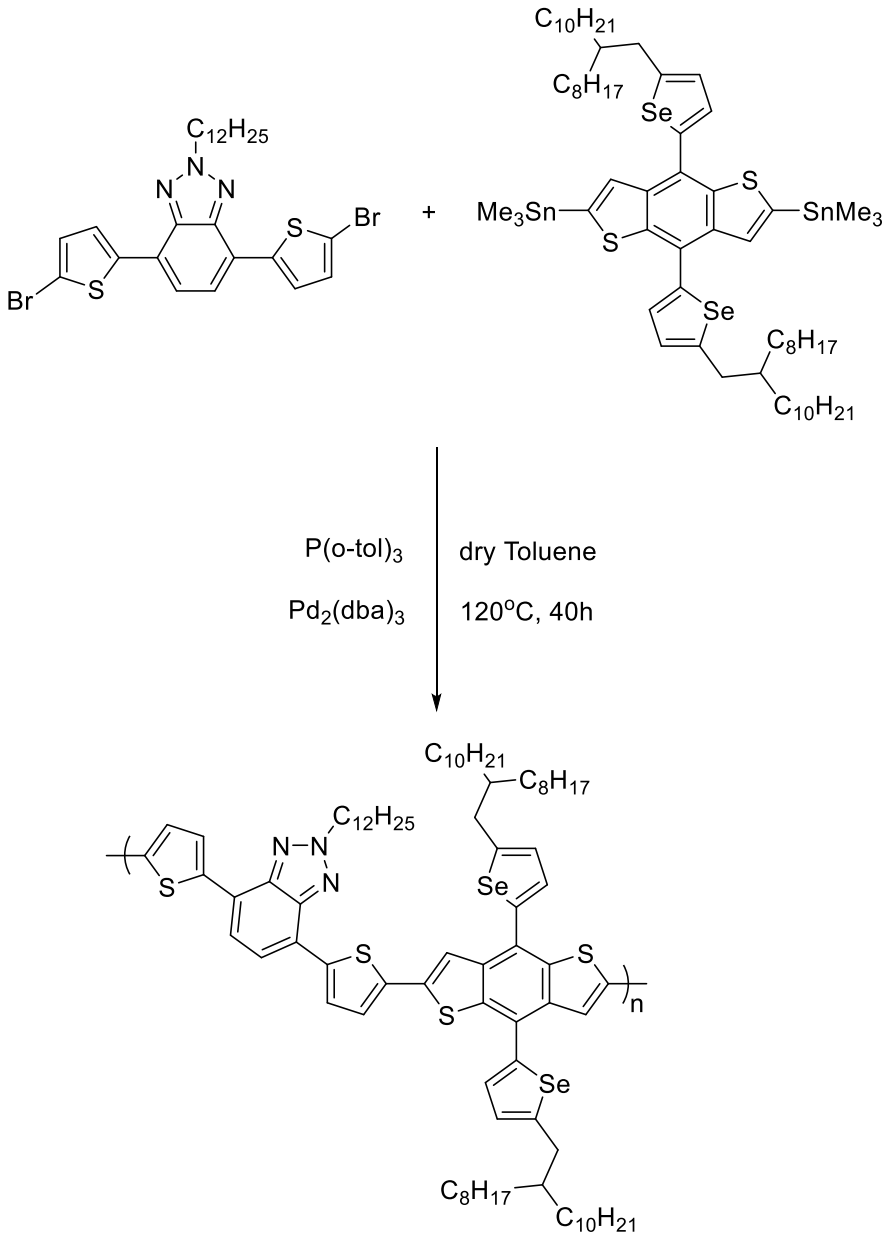

Figure 2.14. Synthesis of **P1**

The monomers 4,7-bis(5-bromothiophen-2-yl)-2-dodecyl-2H-benzo[d][1,2,3]triazole (0.11 g, 0.18 mmol) and (4,8-bis(5-(2-octyldodecyl)selenophen-2-yl)benzo [1,2-b:4,5-b']dithiophene-2,6-diyl)bis(trimethylstannane) (0.24 g, 0.18 mmol) were placed into a 50 mL of two necked rounded reaction flask. Thereafter, freshly distilled toluene (15 mL) was added by syringe to the reaction flask under nitrogen atmosphere and resulting reaction mixture was allowed to be stirred for 30 min. After 30 min, the reaction mixture was purged with nitrogen for another 1 hour. It was followed by the addition of tris(dibenzylideneacetone)dipalladium(0) ($Pd_2(dba)_3$) (8.26 mg, 5% by mol) and tri(*o*-tolyl)phosphine ($P(o\text{-}tol)_3$) (21.97, 40% by mol) to the reaction medium. After that, reaction was allowed to reflux at 120 ^oC for 40 hours under same condition. After 40 hours, 2-bromothiophene (58.85 mg, 0.36 mmol) as a first end-capping group was added, and then, the reaction mixture allowed to be stirried another 4 hours. After 4 hours, 2-tributylstanylthiophene (134.71 mg, 0.36 mmol) utilized as the second end-capping group was added. Then, the reaction mixture was allowed to be refluxed another 5 hours at same temperature. After 5 hours, the reaction mixture was allowed to be cooled down to room temperature. The evaporation of solvent process was achieved under reduced pressure, and the resulting reaction medium was precipitated in cold methanol. After the filtration process of the precipitates, soxhlet extraction was carried out with methanol, acetone, hexane, and chloroform respectively to remove any impurities. Polymer was collected from hexane solvent from soxhlet extraction. Then, evaporation of the solvent was performed under reduced pressure, and the polymer was precipitated in cold methanol one more time. Finally, vacuum filtration method was performed to afford pure dark red polymer product (0.21 g, 80%)

GPC: Mn: 8.2 kDa, Mw: 15.7 kDa, PDI: 1.91

2.3.2. Synthesis of P2

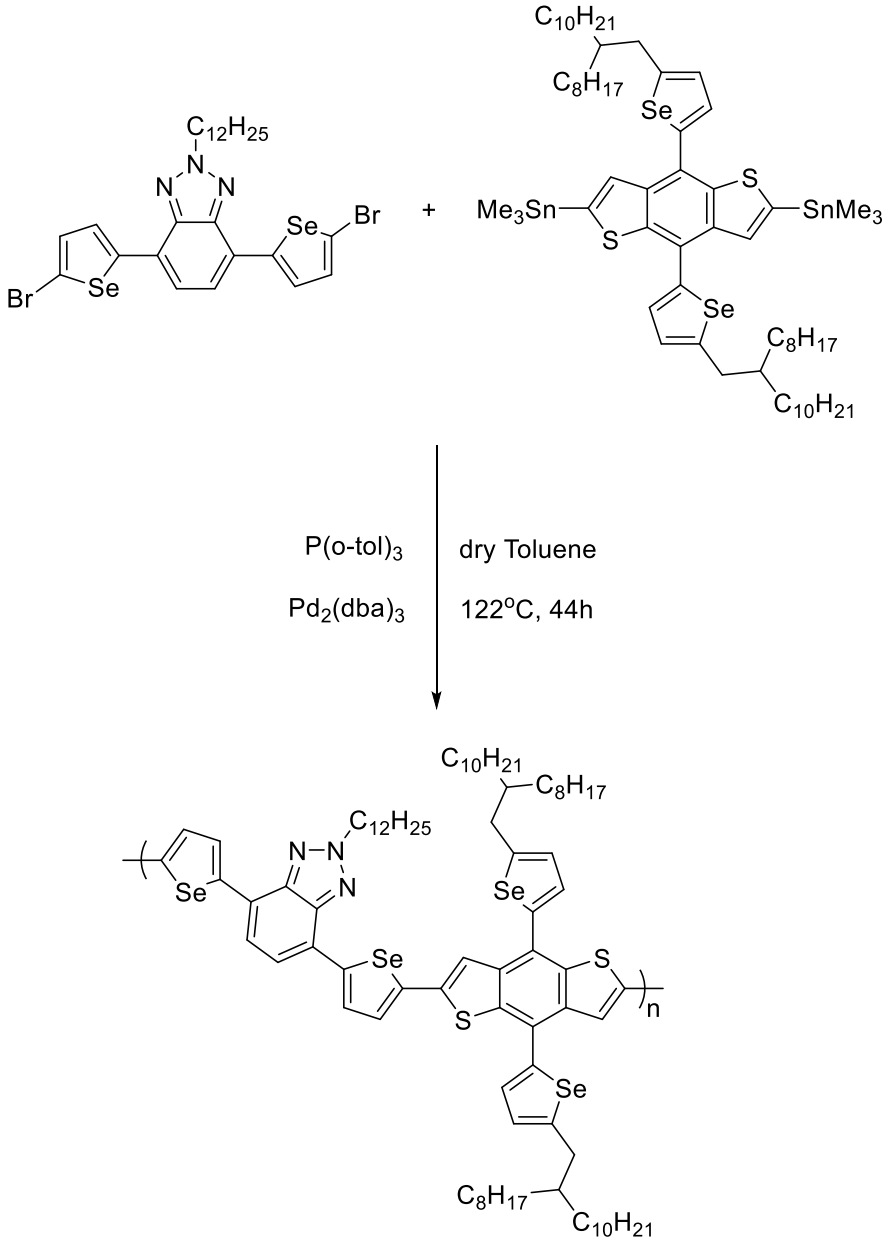

Figure 2.15. Synthesis of **P2**

The monomers 4,7-bis(5-bromoselenophen-2-yl)-2-dodecyl-2H-benzo[d][1,2,3]tri azole (0.12 g, 0.17 mmol) and (4,8-bis(5-(2-octyldodecyl)selenophen-2-yl)benzo[1,2-b:4,5-b']dithiophe- ne-2,6-diyl)bis(trimethylstannane) (0.23 g, 0.17 mmol) were placed into a 50 mL of two necked round reaction flask. After that, freshly distilled toluene (17 mL) was added by syringe into the reaction flask under nitrogen atmosphere, before the mixture was purged with nitrogen for 1 hour. Thereafter, tris(dibenzylideneacetone)dipalladium(0) ($Pd_2(dba)_3$) (7.81 mg, 5% by mol) utilized as catalyst and tri(*o*-tolyl)phosphine ($P(o\text{-}tol)_3$) (20.77, 40% by mol) used as co-catalyst were added to the reaction medium and reaction was allowed to be refluxed at 122 ^oC for 44 hours. After 44 hours, 2-bromothiophene (55.64 mg, 0.34 mmol) utilized as the first end-capping group was added, and the reaction mixture allowed to be stirred another 3 hours. After 3 hours, 2-tributylstanylthiophene (127.35 mg, 0.72 mmol) was added as the second end-capping group. Then, the reaction mixture was allowed to be refluxed another 7 hours at same temperature. After 7 hours, the reaction temperature was reached to the room temperature. The evaporation of solvent process was performed under reduced pressure, before the residual product was precipitated in cold methanol. After filtration of a precipitate, soxhlet extraction was carried out with methanol, acetone, hexane, and chloroform, respectively to eliminate any impurities. Polymer was collected from hexane solvent from soxhlet extraction. Then, evaporation of the solvent process was performed under reduced pressure, and polymer was precipitated in cold methanol one more time. Finally, vacuum filtration technique was performed to afford pure dark violet polymer product. (0.19 g, 72%)

GPC: Mn: 8.1 kDa, Mw: 20 kDa, PDI: 2.47

2.4. Characterization Methods of Conducting Polymers

2.4.1. Gel Permeation Chromatography

The gel permeation chromatography (GPC) technique was carried out to determine the average molecular weight of the synthesized polymers and for calculating their polydispersity index (PDI). The principle behind gel permeation chromatography is

the size or hydrodynamic volume of macro-molecules. Polystyrene standards were utilized in order to calibrate the gel permeation chromatogram.

2.4.2. Electrochemical Studies

To investigate the electrochemical properties of semiconducting polymers, cyclic voltammetry (CV) technique was performed. It is a common way to investigate not only oxidation-reduction behaviors of polymers but also measure HOMO-LUMO energy levels of polymers. Thus, the electronic band gap of a polymer can be determined. To accomplish cyclic voltammetry (CV) studies, potentiostat was utilized with a three-electrode system. In this system, platinum (Pt) wire as the counter electrode (CE), silver (Ag) wire as the reference electrode (RE), and polymer coated indium tin oxide (ITO) as the working electrode were utilized. Gamry Instrument Reference 600 Potentiostat was used to monitor the redox reactions at a constant rate.

2.4.3. Spectroelectrochemical Studies

To gain more in-depth information about changes in electrochromic properties of polymers upon the doping process, spectroelectrochemical studies were carried out by utilizing a three-electrode system presented in the electrochemical cell. Polymers that were dissolved in chloroform solvent were coated on to ITO surface, and subsequently fabricated polymer films were inserted in 0.1 M $TBAPF_6$/ACN electrolyte/solvent couple. The absorption spectrum (UV-Vis-NIR) of polymers provides information about the absorptions of polymers at their neutral states. Moreover, information about polaron and bipolaron bands is obtained from the UV-Vis-NIR absorption spectrum. In addition, color changes of polymers upon electrochemical studies were proved by this spectrum. In addition to these, the optical energy gap (E_g^{op}) of the polymers was measured by utilizing the onset point of the maximum absorption (λ_{onset}), which was determined from the UV-Vis-NIR spectrum.

2.4.4. Kinetic Studies

Kinetic studies were carried out to investigate switching abilities and optical contrast values of resulting polymers between their extreme states by applying voltage at specific wavelengths. Switching times of polymers were evaluated from transmittance change (ΔT%) versus time graph obtained by Chronoamperometry. Besides, optical contrast values of polymers were calculated via UV-Vis-NIR spectrophotometer, which monitored the optical transmittance changes of polymers under an applied voltage.

2.4.5. Thermal Analysis

To investigate the thermal behaviors of synthesized polymers, thermogravimetry analysis (TGA) and differential scanning calorimetry (DSC) were performed. In thermogravimetry analysis (TGA), weight changes of polymers that take place during controlled temperatures in a specific gas atmosphere were quantified. Moreover, changes in physical features of polymers which occur with temperature against time were measured by performing differential scanning calorimetry (DSC).

2.4.6. Photovoltaic Studies

Photovoltaic studies were performed to construct organic solar cell devices and examine the efficiencies of polymers for organic solar cell applications. Bulk hetero-junction type organic solar cells were fabricated with the layers of ITO/PEDOT:PSS/ Polymer:$PC_{71}BM$/LiF/Al, respectively. To construct organic solar cells with this architecture, firstly ITO coated glass substrate acquired from Visiontek Systems, was etched with HCl solution. Then, it was cleaned with toluene, detergent, water, acetone, and isopropyl alcohol, respectively, in the ultrasonic bath for 20 minutes. After the drying process with N_2, oxygen plasma treatment was performed to dispose of any organic impurities on ITO coated glass substrate by using a Harrick Plasma Cleaner. Then, PEDOT:PSS was spin coated on the ITO surface at various rpm rates. After the spin coating process, substrates were dried over to evaporate residual water at 150 ^oC for 15 minutes. Polymer:$PC_{71}BM$ blends, which prepared with different weight ratios,

were filtered with PTFE syringe filter (0.2 μm) to obtain homogenous blends. These fully filtered Polymer:$PC_{71}BM$ blends were spin coated onto the ITO surface in the glove-box, which filled with N_2 (O_2 concentration < 1 ppm, H_2O concentration < 1 ppm). After all, LiF and Al were deposited on the ITO surface by using the thermal evaporation technique. In order to examine J-V characteristics, Keithley 2400 source-meter was used under the illumination of AM 1.5 G.

CHAPTER 3

RESULTS AND DISCUSSION

3.1. Optical Studies of Polymers

The optical studies were conducted to examine the absorption spectrum of resulting polymers **P1** and **P2** in both solution and thin film forms. Recorded UV-Vis spectra of **P1** and **P2** are demonstrated in Figure 3.1 and summary of maximum absorptions in solution, and solid state of **P1** and **P2** is given in Table 3.1. Both polymers showed dual absorption peaks in their thin film forms. The reason for the absorption peak at the shorter wavelength could be the $\pi-\pi^*$ transition in polymer main chains, while the longer wavelength absorption could be attributed to the intramolecular charge transfer (ICT) between donor and acceptor moieties in polymer backbone [69]. Maximum absorption wavelengths were observed as 558 nm with a shoulder at 603 nm for **P1** and 580 nm with a shoulder at 634 nm for **P2** in their thin film forms. In their $CHCl_3$ solutions, maximum wavelengths were recorded as 512 nm for **P1** and 528 nm for **P2**.

Table 3.1. Summary of optical studies for **P1** and **P2**

Polymer	Solution λ_{max} (nm)	Thin Film λ_{max} (nm)
P1	512	558/603
P2	528	586/634

Shifts towards the longer wavelengths at maximum absorption peaks of both polymers were observed from their dilute chloroform solution forms to the thin film states. Due to decreases in conformational freedom and interactions between solvent and polymer, and also increase in the tendency to aggregation between polymer chains in the solid

state, usually a red-shifted absorption appear in thin film form in comparison with solution form [70], [71]. Moreover, maximum absorption of **P2** shifts toward longer wavelengths, which is known as red shift compared with **P1**, was observed. This observation could be resulted from the stronger interactions in the selenophene containing **P2** than thiophene containing **P1** since selenium atom is polarized easier than sulfur atom [72].

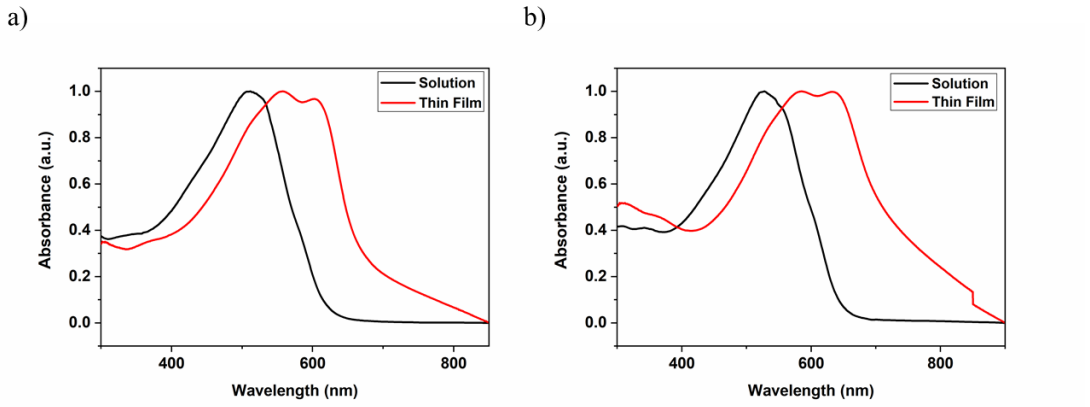

Figure 3.1. UV-Vis absorption spectra of a) **P1** and b) **P2** presented in $CHCl_3$ solution and solid state

3.2. Electrochemical Studies of Polymers

The cyclic voltammetry (CV) technique was performed to deeply investigate the electrochemical properties of synthesized polymers. HOMO and LUMO energy levels of the polymers were calculated by resulting cyclic voltammograms, as well as the redox behaviors of the polymers were investigated. Therefore, the electronic band gap of polymers was calculated by using their defined HOMO and LUMO levels. To achieve electrochemical studies, Gamry Instrument Reference 600 Potentiostat, which was used to monitor the redox reactions at a constant rate, was utilized with a

three-electrode configuration. In this system, platinum (Pt) wire, silver (Ag) wire, and polymer coated indium tin oxide (ITO) were used as the counter (CE), reference (RE), and working electrodes (WE) respectively. To accomplish the cyclic voltammetry studies, polymer solutions in chloroform (5mg/mL) were spray coated onto ITO coated glass surface. Then, it was immersed in the 0.1 M $TBAPF_6$/ACN electrolyte solution presented in the quartz cuvette. Also, Pt and Ag wires were immersed in this cuvette. Cyclic voltammograms were recorded between controlled potentials for resulting polymers **P1** and **P2** with a 100 mV/s scan rate at room temperature. As demonstrated in Figure 3.2, cyclic voltammograms exhibited that **P1** and **P2** possess both p-dopable and n-dopable features, which is known as ambipolar character. For **P1** and **P2**, both oxidation and reduction potentials were recorded, and their onset potentials were evaluated from cyclic voltammograms.

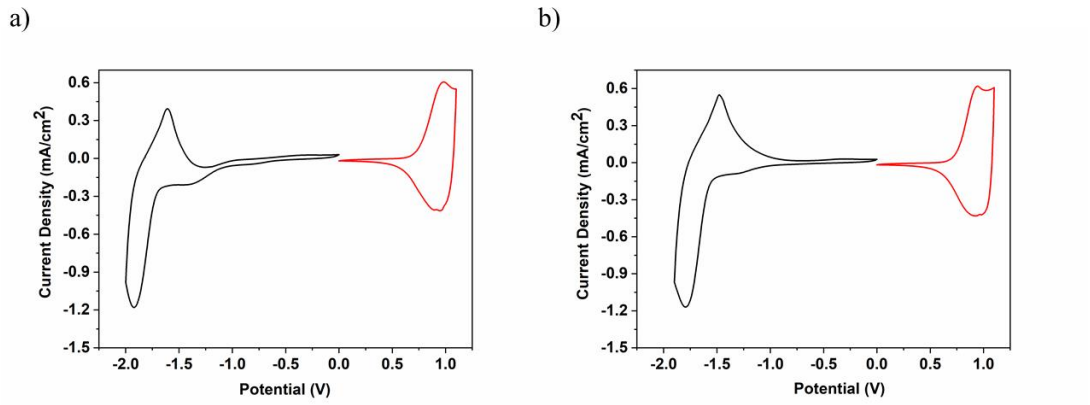

Figure 3.2. Cyclic voltammograms of thin film of a) **P1** and b) **P2** in 0.1 M $TBAPF_6$/ACN solution

The reversible p-type doping/dedoping couple potentials of **P1** and **P2** were recorded at 0.98 V/ 0.89 V and 0.94 V/ 0.91 V, respectively. In addition, the reversible n-type

doping/dedoping couple peaks of **P1** and **P2** were observed at -1.92 V/ -1.61 V and -1.79 V/ -1.47 V, respectively. According to these results, the oxidation potential of **P1** is relatively higher than **P2**. Lower oxidation potential of **P2** could be correlated with the increase in the electron density on the polymer backbone, which resulted from stronger electron donating feature of selenophene than thiophene [73].

Since both polymers have ambipolar character, their HOMO and LUMO energy levels were calculated utilizing their onset of oxidation and reduction potentials. Following equations were used where standard hydrogen electrode (SHE) versus vacuum level was taken as 4.75 eV;

$$HOMO = -(4.75 + E_{ox}^{onset})$$

$$LUMO = -(4.75 + E_{red}^{onset})$$

The electronic band gap (E_g^{el}) of polymers was deduced from the difference between HOMO and LUMO energy levels. Therefore, electronic band gaps of **P1** and **P2** were calculated by using the following equation;

$$E_g^{el} = HOMO - LUMO$$

The HOMO energy level measurements were recorded as -5.45 V and -5.49 V for **P1** and **P2**, respectively, by using their oxidation potential onset values, while the measurements of LUMO energy levels were recorded as -3.09 V and -3.21 V, in order of **P1** and **P2**. Hence, the corresponding electronic band gap (E_g^{el}) values were calculated as 2.36 eV and 2.28 eV for **P1** and **P2**, respectively. The electrochemical properties of **P1** and **P2** were summarized in Table 3.2. Upon cyclic voltammetry results, selenophene containing polymer **P2** possesses a lower band gap compared to that of thiophene based polymer **P1**. Literature studies have shown that introducing selenophene unit in the conjugated polymer main chain instead of thiophene analogs decreases the electronic band gap of polymer, owing to provide deeper LUMO level without any change in HOMO energy level. Higher polarizability of selenium atom

than sulfur atom could be attributed to the deeper LUMO level of selenophene bearing polymers [74]–[76].

Table 3.2. Summary of electrochemical properties of **P1** and **P2**

Polymer	$E_{p\text{-doping}}$ (V)	$E_{p\text{-dedoping}}$ (V)	$E_{n\text{-doping}}$ (V)	$E_{n\text{-dedoping}}$ (V)	HOMO (eV)	LUMO (eV)	E_g^{el} (eV)
P1	0.98	0.89	-1.92	-1.61	-5.45	-3.09	2.36
P2	0.94	0.91	-1.79	-1.47	-5.49	-3.21	2.28

3.3. Spectroelectrochemical Studies of Polymers

Spectroelectrochemical measurements of **P1** and **P2** were conducted to examine information about variances in electrochromic and optical features of polymers upon applied different potentials. To prepare the working electrodes (WE) utilized in spectroelectrochemical studies, polymers were dissolved in chloroform solvent with 3mg/mL before polymer/solvent solution were spray coated onto the ITO surface. Then polymer films were immersed in the 0.1 M TBAPF6/ACN electrolyte solution presented in an electrochemical cuvette, and UV-Vis-NIR absorption spectra of **P1** and **P2** were recorded under steadily increasing potential from 0.0 V to 1.2 V.

As seen in Figure 3.3, maximum absorptions were observed at 558 nm and 603 nm with an onset of the maximum absorption peak at 723 nm in the visible region for **P1**, while **P2** exhibited relatively red shifted maximum absorptions point at 580 nm and 634 nm with an absorption onset at 846 nm in the visible region. Red shifted maximum absorption of **P2** could result from the stronger interactions of polymer main chain which has selenophene moiety as a π-bridge [72]. Maximum absorptions in the visible region could be attributed to π-π* electronic transitions that occurred between HOMO and LUMO energy levels of conjugated polymers [71].

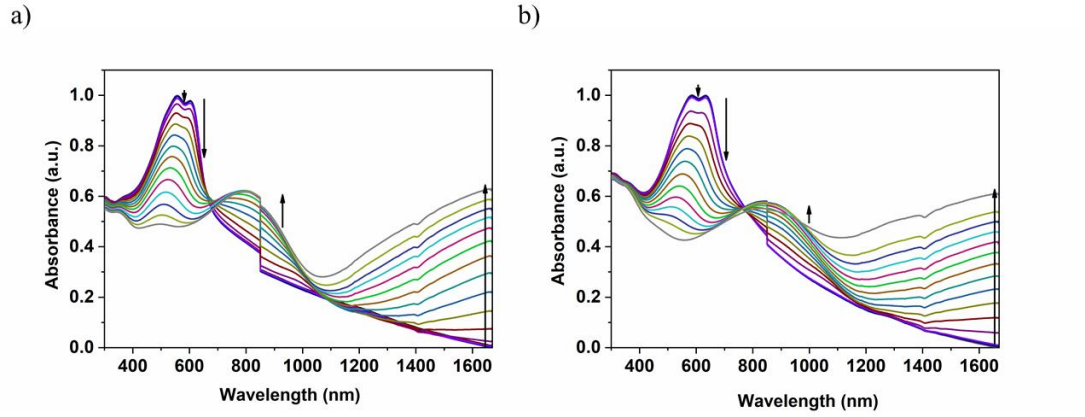

Figure 3.3. UV-Vis-NIR absorption spectra of thin film of a) **P1** and b) **P2** in 0.1 M $TBAPF_6$/ACN electrolyte/solvent couple

With increasing potential, the absorptions in the visible region began to decrease concurrently, and formation of polaron bands became intensified at approximately 805 nm and 830 nm for the resulting polymers **P1** and **P2**, respectively. Generation of polaron band could be correlated to reduce in concentration of neutral polymer by increasing applied potential resulting in enhancement of polaron species concentration. With a further increase in potential, another band called bipolaron band became intensified at around 1635 nm and 1620 nm in the NIR region for the polymers **P1** and **P2**, respectively. Formation of these bands in absorption spectra exhibited that as continuous to apply external voltage, oxidation of polymers proceeded, and generation of lower energy charge carriers such as polarons and bipolarons started [69].

The optical band gap (E_g^{op}) were estimated from the onset point of absorption maxima in the UV-Vis-NIR absorption spectrum of the polymer thin film by utilizing the following equation;

$$E_g^{op} = \frac{1241}{\lambda_{max}^{onset}}$$

Calculations of the optical band gap energies of polymers were recorded as 1.72 eV and 1.47 eV for the resulting polymers **P1** and **P2**, respectively. Selenophene containing polymer **P2** possesses a lower band gap than polymer **P1,** which has a thiophene unit in its backbone. The decrease in the band gap of selenophene based polymer compared with thiophene based polymer could be correlated with a more electron rich nature and more quinoidal character of selenophene. Lower band gap polymers have advantages of more light absorption [76], [77]. Summary of the spectroelectrochemical features of **P1** and **P2** are demonstrated in Table 3.3.

Table 3.3. Summary of spectroelectrochemical properties of **P1** and **P2**

Polymer	λ_{max} (nm)	λ_{max}^{onset} (nm)	E_g^{op} (eV)
P1	558/603	723	1.72
P2	580/634	846	1.47

Colors of the polymers **P1** and **P2** were monitored under different applied potential. In addition to this, their colors were classified by the International Commission on Illumination (CIE) system. The CIE system is depended on three main parameters which are abbreviated as 'L', 'a' and 'b'. While 'L' value stands for the lightness information, 'a' and 'b' values present the red to green and blue to yellow scales, respectively. Both colors and L, a, b values of **P1** and **P2** are demonstrated in Figure 3.4. The thin film of **P1** at neutral state exhibited the violet color (L: 10.5, a: 1.8, b: -1.1), while it exhibited the brownish-green color (L: 14.0, a: -5.8, b: 9.1) in reduction state and it possessed the grayish-blue color (L: 14.6, a: -3.1, b: -8.2) in oxidation state. The color of **P2** film was dark violet (L: 9.6, a: 1.3, b: -1.7) in neutral state, whereas its color shifted the grayish-blue (L: 15.2, a: -4.7, b: -4.8) in oxidation state and

grayish-green (L: 15.9, a: -4.9, b: 3.7) in reduction state by the way of changing the applied potential.

a)

-2.0 V	0.0 V	1.2 V
		
L= 14.0 a= -5.8 b= 9.1	L= 10.5 a= 1.8 b= -1.1	L= 14.6 a= -3.1 b= -8.2

b)

-2.0 V	0.0 V	1.2 V
		
L= 15.9 a= -4.9 b= 3.7	L= 9.6 a= 1.3 b= -1.7	L= 15.2 a= -4.7 b= -476

Figure 3.4. Colors and L,a,b values of thin film of a) ***P1*** and b) ***P2*** under -2.0 V, 0.0 V and 1.2 V, respectively

3.4. Kinetic Studies of Polymers

To probe the switching times and optical contrast values of the polymers **P1** and **P2,** kinetic studies were achieved by applying the square-wave voltammetry. The percent transmittance change at specific wavelengths is known as the optical contrast. Optical contrast values (ΔT%) of polymers at specific wavelengths were recorded by applying regular alternating potentials in between neutral states and oxidized states of **P1** and **P2**. These studies were carried out by a UV-Vis-NIR spectrophotometer with the 5 s time intervals. Switching time is basically described as the time required to switch between two extreme states. Chronoamperometry was utilized to record response times of polymers evaluated from transmittance change (ΔT%) versus time graph, as depicted in Figure 3.5.

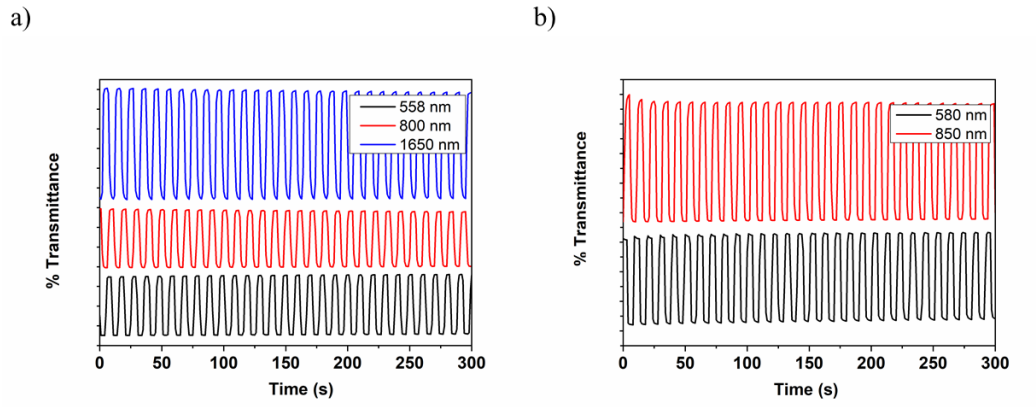

Figure 3.5. Changes in percent transmittance of the thin film of a) **P1** and b) **P2** in 0.1 M $TBAPF_6$/ACN electrolyte/solvent couple

Optical contrast values of **P1** were recorded as 30% at 558 nm and 30% at 800 nm in the visible region and 56% at 1650 nm in the NIR region with the switching times of 1.9 s, 1.9 s, and 1.7 s, respectively. **P1** exhibited the highest optical contrast as 56% and the lowest response time values as 1.7 s at its maximum wavelength in the NIR region. For **P2**, optical contrast ($\Delta T\%$) values were found as 30% at 580 nm and 41% at 850 nm in the visible region. Switching times of **P2** were recorded as 1.4 s and 0.9 s at 580 nm and 850 nm, respectively. The summary of kinetic studies of polymers is demonstrated in Table 3.4.

Table 3.4. Summary of kinetic studies of **P1** and **P2**

Polymer	Wavelength (nm)	Optical Contrast (ΔT%)	Switching Time (s)
	558	30	1.9
P1	800	30	1.9
	1650	56	1.7
P2	580	30	1.4
	850	41	0.9

3.5. Thermal Analysis of Polymers

To investigate the weight changes of polymers, thermogravimetry analysis (TGA) was performed by Perkin Elmer Pyris 1 TGA device under the nitrogen atmosphere. All TGA analyses were carried out with a heating rate of 10 °C/min at a temperature range between 25 °C and 600 °C. TGA results show that weight losses of **P1** and **P2** started at 370 °C and 375 °C, respectively. 57% weight loss of **P1** was observed until 530 °C, while 70% weight loss of **P2** was observed until 500 °C, which could be caused from the covalent bonds detaching on the main chain of the polymer.

To investigate the thermal transition properties of polymers, differential scanning calorimetry (DSC) was performed by Perkin Elmer DSC 8000 device under the nitrogen atmosphere. All DSC measurements were conducted with the 10 °C/min heating rate at a temperature between 25 °C and 300 °C. DSC results demonstrated that glass transition temperatures (T_g) of **P1** and **P2** could not be observed. The reason for this might be that synthesized polymers possess rigid structures in their main chains. All TGA and DSC graphs were given in Appendix B.

3.6. Organic Solar Cell Applications of Polymers

Organic bulk heterojunction solar cell applications were conducted by utilizing the sandwich device construction of ITO/PEDOT:PSS/Polymer:$PC_{71}BM$/LiF (0.7nm)/Al

(100nm). Synthesized polymers **P1** and **P2** were introduced as donor materials, and $PC_{71}BM$ utilized as the acceptor material in the active layers of constructed devices. Convenient energy levels presented between device components are crucial parameter for obtaining high-performance solar cells. Energy level profiles of **P1** and **P2** containing organic solar device was illustrated in Figure 3.6. Information about HOMO and LUMO energy levels of polymers were provided from cyclic voltammetry studies that were mentioned in the Section 3.2. This energy levels illustration ensured that both polymers were suitable to be utilized as donor materials for the ITO/PEDOT:PSS/Polymer:$PC_{71}BM$/LiF/Al bulk heterojunction solar cell device architecture.

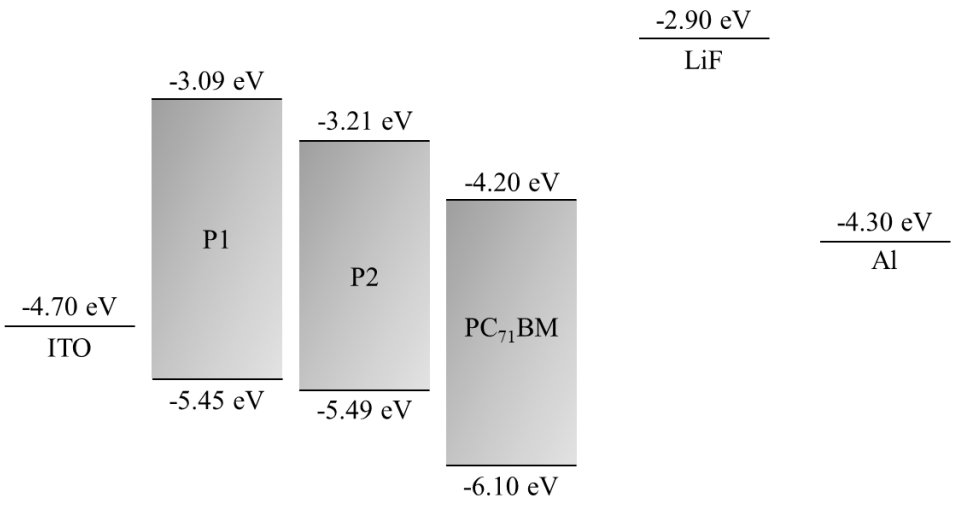

Figure 3.6. Energy level profiles of **P1** and **P2** based bulk heterojunction solar cell construction

Several optimization studies, including various polymer:$PC_{71}BM$ ratio (w/w), blend concentration, active layer thickness, and utilizing of additives, were performed to reach the best performances of organic solar cells. All optimization variables affect

the parameters that have a crucial role in the efficiencies of OSCs, including V_{OC}, J_{SC}, and fill factor. In addition to these varied optimization techniques, the effects of different solvents usage on the device performance were investigated. Enhancing solubility of polymer by proper choice of solvent improves both exciton dissociation and charge carrier transport property due to present better morphology [78], [79]. For this reason, chloroform, chlorobenzene, and chlorobenzene: orthodichlorobenzene (1:1) (v/v) were utilized during OSCs construction. For both **P1** and **P2** based devices, chlorobenzene: orthodichlorobenzene (1:1) solvent mixture exhibited the best performance.

Current density (mA/cm^2) – voltage (V) graphs were demonstrated in Figure 3.7 and Figure 3.7 for **P1** and **P2**, respectively. They clearly showed how the optimization studies affect the V_{OC}, J_{SC}, and fill factor of devices as well as power conversion efficiencies.

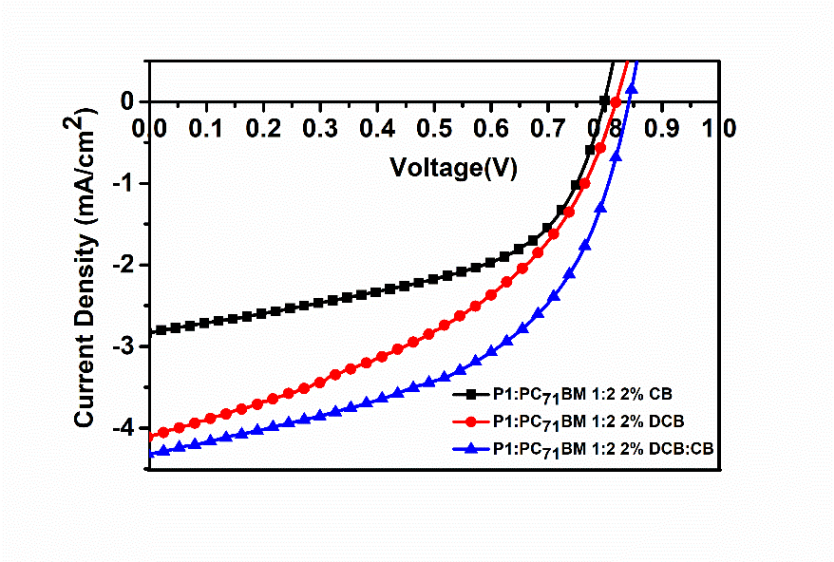

Figure 3.7. Current density-voltage curves of OSCs based on **P1**:$PC_{71}BM$ (1:2) blend with different solvents

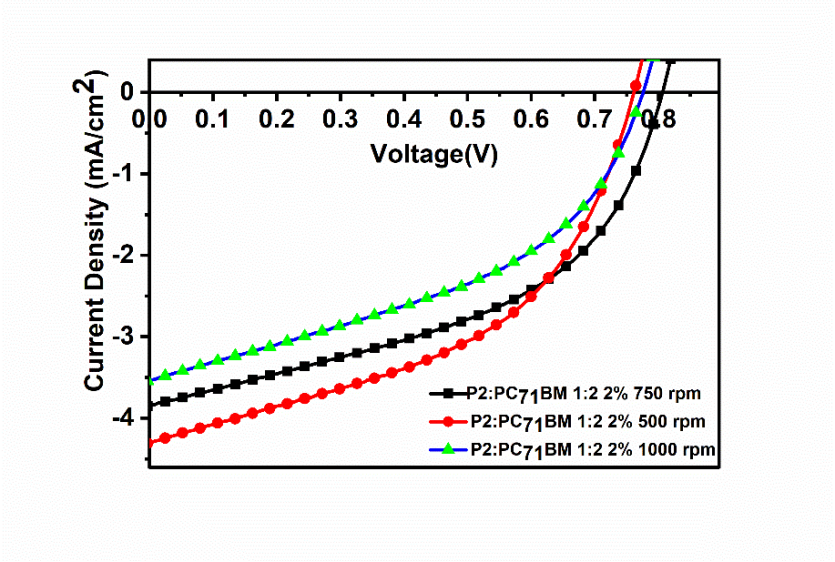

Figure 3.8. Current density-voltage curves of OSCs based on **P2**:$PC_{71}BM$ (1:2) blend with different active layer thicknesses

After different polymer: $PC_{71}BM$ (w/w) ratios were investigated in the active layer of OSC devices, 1:2 polymer: $PC_{71}BM$ blend ratio exhibited the best efficiency for both **P1** and **P2**. Blend ratio optimization is one of the most important factors influencing the power conversion efficiency of OSCs. By increasing the amount of electron accepting material $PC_{71}BM$ in the donor-acceptor blend, negative charge carrier transport features are enhanced. The role of acceptor material is mostly related to the charge transport in the active layer. This enhancement in electron transportation leads to obtain effective charge separation and a higher amount of collection of separated charge carriers to the proper electrodes; therefore, enhancement in device efficiency was observed. However, an increase in $PC_{71}BM$ amount in the donor-acceptor blend results in decreasing donor material that is responsible for the absorption of light in the active layer. The reduction of efficient light absorption resulting in lower short circuit current of device causes to obtain low power conversion efficiency. Thus, determining the optimum polymer: $PC_{71}BM$ blend ratio in active layer of devices is a crucial parameter for obtaining high-performance solar cells.

Another variable that was optimized to obtain high PCE is the concentration ratio (w/v) between donor-acceptor blend and utilized solvent. Both **P1** and **P2** based OSC devices exhibited their best performances in 2% blend concentration. In higher blend concentrations, too much closely packed donor and acceptor molecules in the active layer were observed. This tightly packing morphology causes the decrease in the desired phase separation in the active layer, and thus increase in PCE of device is observed.

Optimizations of active layer thickness of both **P1** and **P2** containing devices were performed by altering spin coating rates. As the spin rate decreases, the thickness of the active layer increases. In order to obtain more light absorption, a thicker active layer film is needed. However, thicker films might cause undesired recombination process due to possessing long distance for charge carrier transportation. In addition to this, an unenviable situations such as low R_{SH} and high R_S could result from a thicker active layer film [80]. Optimum spin rate was found as 1000 rpm and 500 rpm for **P1** and **P2**, respectively.

Additive treatments were performed by the addition of 2% DIO -diiodooctane- for both **P1** and **P2** based devices. However, the reduction in PCE of both polymers **P1** and **P2**. Moreover, the addition of 3% DPE -diphenyl ether- was performed for both polymers. However, decreases in device performances were observed for **P1** and **P2** containing OSC devices. This might result from the good interactions of additives with donor and acceptor materials could not be achieved.

Summaries of photovoltaic studies of **P1** and **P2** were demonstrated in Table 3.5 and 3.6, respectively.

Table 3.5. Summary of photovoltaic studies of **P1** utilized bulk heterojunction solar cells

P1:$PC_{71}BM$	Solvent	J_{sc} (mA/cm^2)	V_{oc} (V)	FF (%)	η (%)	RPM	Treatment
1:1 (2%)	CB	2.45	0.73	33.60	0.60	750	-
1:2 (2%)	CB	2.83	0.80	52.32	1.18	750	-
1:3 (2%)	CB	1.12	0.70	19.42	0.15	750	-
1:4 (2%)	CB	0.97	0.74	43.20	0.31	750	-
1:2 (2%)	DCB	4.10	0.83	42.54	1.44	750	-
1:2 (2%)	CB:DCB	4.32	0.85	50.47	1.84	750	-
1:2 (1%)	CB:DCB	2.22	0.72	58.06	0.93	750	-
1:2 (3%)	CB:DCB	2.40	0.83	47.37	0.94	750	-
1:2 (2%)	CB:DCB	4.17	0.84	50.80	1.78	500	-
1:2 (2%)	CB:DCB	5.66	0.83	51.22	2.41	1000	-
1:2 (2%)	CB:DCB	3.54	0.87	45.78	1.41	1000	2% DIO
1:2 (2%)	CB:DCB	4.92	0.84	49.54	2.04	1000	3% DPE

Table 3.6. Summary of photovoltaic studies of **P2** utilized bulk heterojunction solar cells

P2:$PC_{71}BM$	Solvent	J_{sc} (mA/cm^2)	V_{oc} (V)	FF (%)	η (%)	RPM	Treatment
1:1 (2%)	CB	2.36	0.79	33.61	0.62	750	-
1:2 (2%)	CB	2.87	0.73	46.23	0.97	750	-
1:3 (2%)	CB	3.16	0.73	39.08	0.90	750	-
1:4 (2%)	CB	1.98	0.72	46.52	0.66	750	-
1:2 (2%)	DCB	4.30	0.75	42.03	1.35	750	-
1:2 (2%)	CB:DCB	3.84	0.81	46.97	1.46	750	-
1:2 (1%)	CB:DCB	1.35	0.63	53.81	0.46	750	-
1:2 (3%)	CB:DCB	2.17	0.80	45.07	0.79	750	-
1:2 (2%)	CB:DCB	4.30	0.77	47.37	1.56	500	-
1:2 (2%)	CB:DCB	4.80	0.74	34.49	1.22	1000	-
1:2 (2%)	CB:DCB	3.59	0.80	41.68	1.20	1000	2% DIO
1:2 (2%)	CB:DCB	3.44	0.80	46.18	1.28	1000	3% DPE

According to the results of photovoltaic studies, best power conversion efficiency was achieved as 2.41% for the device containing P1:$PC_{71}BM$ (1:2) (w/w) in CB-DCB (1:1) (v/v) solvent ratio. For this device, V_{OC}, J_{SC}, and FF values were recorded as 0.83 V, 5.66 mA/cm^2, and 51.22%, respectively. For **P2** based OSC devices, best efficiency was observed as 1.56% for the blend ratio as P2:$PC_{71}BM$ (1:2) (w/w) in CB-DCB (1:1) (v/v) with the V_{OC}, J_{SC} and FF values as 0.77 V, 4.30 mA/cm^2 and 47.37%, respectively.

The reason for exhibiting lower PCE of devices that contain selenophene based **P2** than thiophene based polymer **P1** could be that selenophene based polymers mostly possess lower the molar absorption coefficients resulting in lower light absorption.

This issue reveals that selenophene containing polymers exhibit lower J_{SC} values than thiophene based polymer analogs. Moreover, selenophene bearing polymers possess relatively lower positive charge carrier mobilities resulting in thinner active layer needed. This might cause comparatively lower efficiencies for selenophene bridged polymers **P2** based solar cells.

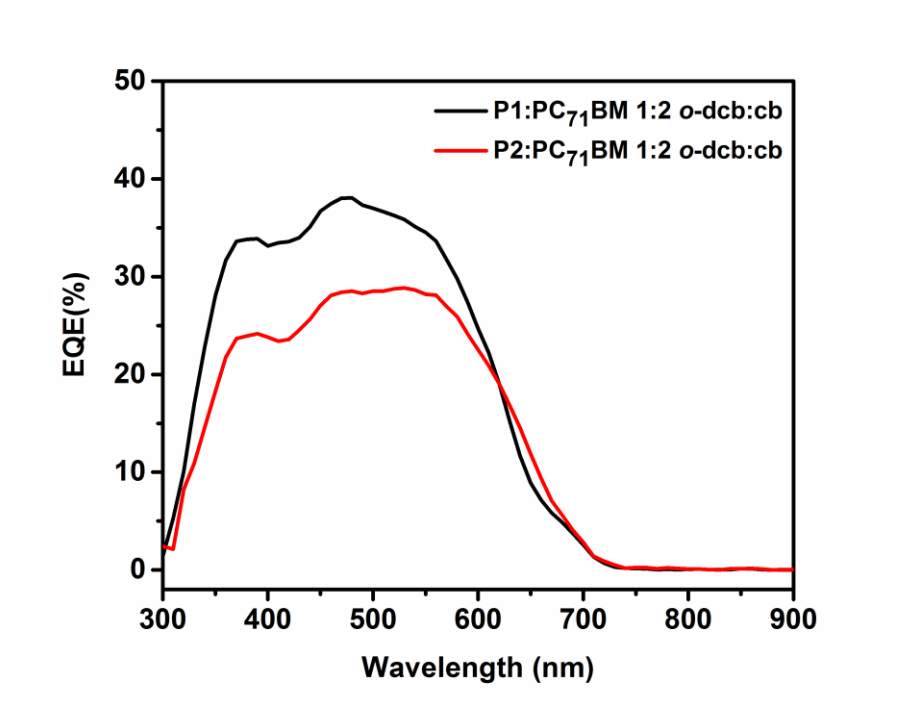

Figure 3.9. EQE curves of OSCs incorporating **P1**:$PC_{71}BM$ (1:2) and **P2**:$PC_{71}BM$ (1:2) blends

External quantum efficiency (EQE) of P1 and P1 corporate devices were recorded from incident photon to converted electron (IPCE) ratios. As depicted in Figure 3.9, External quantum efficiencies of the **P1** and **P2** based solar cells, which exhibited the high performances, were recorded as 38% and 28%, respectively.

3.7. Morphology Analysis of Polymers

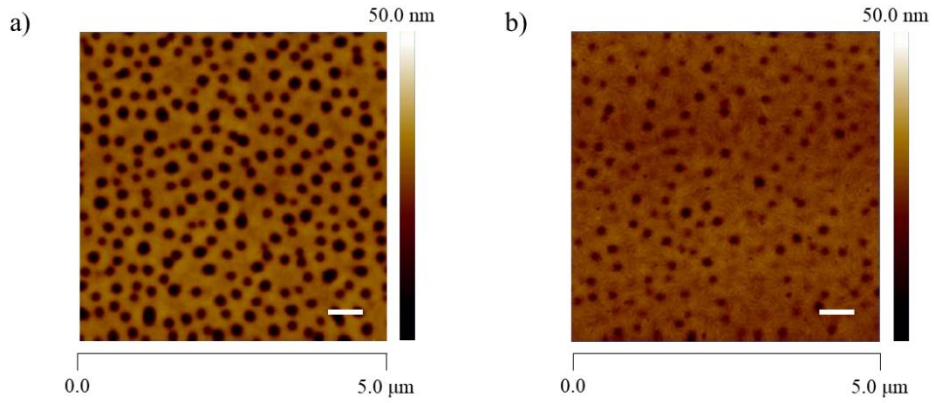

Figure 3.10. AFM topography images of a) **P1**:$PC_{71}BM$ (1:2) 2% constructed with CB:DCB (1:1) and b) **P2**:$PC_{71}BM$ (1:2) 2% constructed with CB:DCB (1:1). Scale bar is 200 nm.

Atomic force microscopy analyses were conducted to obtain topography information of **P1** and **P2** based solar cells, which exhibited the best performance among utilized several optimizations. AFM images of the active layers of the **P1** and **P2** based devices with the best performances were shown in Figure 3.10. According to AFM analyses, surface roughness and thickness of P1:$PC_{71}BM$ (1:2) containing active layer was recorded as 4.62 nm and 110 nm, respectively. For the active layer of P2:$PC_{71}BM$ (1:2) containing solar cell, surface roughness, and thickness were examined as 110 nm and 75 nm, respectively.

CHAPTER 4

CONCLUSION

Two donor-acceptor type alternating polymers having benzotriazole based acceptor moiety and benzodithiophene based donor moiety with different π-bridge groups were synthesized via Stille coupling reaction. Thiophene and selenophene molecules were utilized as π-bridge groups for **P1** and **P2**, respectively. Synthesized polymers were used as electron rich donor moieties for bulk heterojunction organic solar cells. Gel permeation chromatography results exhibited that **P1** and **P2** possess 8.2 kDa and 8.1 kDa number average molecular weights, respectively. Both polymers exhibited broad absorptions in the visible region, according to UV-Vis absorption spectra. Maximum absorption of **P2** shifts toward longer wavelengths, due to possessing selenophene π-bridge in its backbone. Spectroelectrochemical properties of **P1** and **P2** were determined via UV-Vis-NIR absorption spectroscopy. In accordance with UV-Vis-NIR absorption spectra of polymers, maximum absorption points were recorded as 558/603 nm and 580/634 nm for **P1** and **P2**, respectively. Moreover, maximum absorption onset values of polymers were determined as 723 nm for **P1** and 846 nm for **P2**. Therefore, optical band gap values of **P1** and **P2** were calculated as 1.72 eV and 1.47 eV, respectively. The reason of possessing energetically lower band gap of **P2** is electron rich nature and more quinoidal character of selenophene. Cyclic voltammetry studies were conducted to clarify the electrochemical features of polymers. HOMO and LUMO energy levels were determined as -5.45/ -3.09 eV and -5.49/ -3.21 eV for **P1** and **P2**, respectively. Electronic band gap values of **P1** and **P2** were recorded as 2.36 eV and 2.28 eV, correspondingly. Selenophene incorporated **P2** possesses lower band gap than thiophene based **P1**, due to higher polarizability of selenium atom than sulfur atom might be attributed to the deeper LUMO level of selenophene bearing polymers. These energy levels ensured that both polymers were

suitable to be utilized as donor materials for the bulk heterojunction solar cell device. Kinetic studies showed that maximum optical contrast values were determined as 56% at 1650 nm with the switching time of 1.7 s for **P1** and 41% at 850 nm with the 0.9 s switching time for **P2**.

Both polymers were utilized as an electron rich donor moieties for the bulk heterojunction organic solar cells with the ITO/PEDOT:PSS/Polymer:$PC_{71}BM$/LiF (0.7 nm)/Al (100 nm) device architecture. In accordance with the photovoltaic studies, best power conversion efficiency was achieved as 2.41% for **P1** incorporated solar cell device with the V_{OC}, J_{SC}, and FF values as 0.83 V, 5.66 mA/cm^2, and 51.22%, respectively. **P2** based OSC devices exhibited the best power conversion efficiency as 1.56% with the V_{OC}, J_{SC} and FF values as 0.77 V, 4.30 mA/cm^2 and 47.37%, respectively.

REFERENCES

[1] A. K. Mishra, "Conducting Polymers: Concepts and Applications," *J. At. Mol. Condens. Nano Phys.*, vol. 5, no. 2, pp. 159–193, 2018.

[2] Y. Li, "Organic Optoelectronic Materials," in *Organic Optoelectronic Materials*, vol. 91, no. 1, 2015, pp. 23–50.

[3] A. Facchetti, "π-Conjugated polymers for organic electronics and photovoltaic cell applications," *Chem. Mater.*, vol. 23, no. 3, pp. 733–758, 2011.

[4] M. A. Rahman, P. Kumar, D. S. Park, and Y. B. Shim, "Electrochemical sensors based on organic conjugated polymers," *Sensors*, vol. 8, no. 1, pp. 118–141, 2008.

[5] X. Guo, M. Baumgarten, and K. Müllen, "Designing π-conjugated polymers for organic electronics," *Prog. Polym. Sci.*, vol. 38, no. 12, pp. 1832–1908, 2013.

[6] E. Saion, A. Kassim, N. Yahya, and M. Hamzah, "Conjugated Conducting Polymers : A Brief Conjugated Conducting Polymers : A Brief Overview," *J. Am. Stat. Assoc.*, no. June, 2007.

[7] A. G. MacDiarmid, "'Synthetic Metals,'" *Angew. Chemie*, vol. 40, no. 14, pp. 2581–2590, 2001.

[8] B. Lüssem, M. Riede, and K. Leo, "Doping of organic semiconductors," *Phys. Status Solidi Appl. Mater. Sci.*, vol. 210, no. 1, pp. 9–43, 2013.

[9] R. Fujimoto, Y. Yamashita, S. Kumagai, and J. Tsurumi, "Molecular doping in organic semiconductors: Fully solution-processed, vacuum-free doping with metal-organic complexes in an orthogonal solvent," *J. Mater. Chem. C*, vol. 5, no. 46, pp. 12023–12030, 2017.

[10] M. A. De Paoli and W. A. Gazotti, "Electrochemistry, polymers and opto-electronic devices: A combination with a future," *J. Braz. Chem. Soc.*, vol. 13, no. 4, pp. 410–424, 2002.

[11] A. K. Bakhshi and G. Bhalla, "Electrically conducting polymers: Materials of the twentyfirst century," *J. Sci. Ind. Res. (India).*, vol. 63, no. 9, pp. 715–728, 2004.

[12] D. Liming, *Intelligent Macromolecules for Smart Devices From Materials Synthesis to Device Applications*. 2004.

[13] C. Liu, K. Wang, X. Gong, and A. J. Heeger, "Low bandgap semiconducting polymers for polymeric photovoltaics," *Chem. Soc. Rev.*, vol. 45, no. 17, pp. 4825–4846, 2016.

[14] Y. J. Cheng, S. H. Yang, and C. S. Hsu, "Synthesis of conjugated polymers for organic solar cell applications," *Am. Chem. Soc.*, vol. 109, no. 11, pp. 5868–5923, 2009.

[15] X. D. Xie and D. Lu, "Energy Band Theory of Solids," *Electron. Eng. Mater. Nanotechnol.*, no. December, pp. 307–432, 2007.

[16] P. Yu and M. Cardona, *Fundamentals of Semiconductors: Physics and Materials Properties*, 3rd ed., no. December 2014. 2003.

[17] C. L. Chochos and S. A. Choulis, "How the structural deviations on the backbone of conjugated polymers influence their optoelectronic properties and photovoltaic performance," *Prog. Polym. Sci.*, vol. 36, no. 10, pp. 1326–1414, 2011.

[18] Y. J. Cheng, S. H. Yang, and C. S. Hsu, "Synthesis of conjugated polymers for organic solar cell applications," *Am. Chem. Soc.*, vol. 109, no. 11, pp. 5868–5923, 2009.

[19] G. L. Gibson, T. M. McCormick, and D. S. Seferos, "Atomistic band gap engineering in donor-acceptor polymers," *J. Am. Chem. Soc.*, vol. 134, no. 1, pp. 539–547, 2012.

[20] J. Warnan, A. El Labban, C. Cabanetos, and E. T. Hoke, "Ring substituents mediate the morphology of PBDTTPD-PCBM bulk-heterojunction solar cells," *Chem. Mater.*, vol. 26, no. 7, pp. 2299–2306, 2014.

[21] D. Gedefaw, M. Tessarolo, and M. Bolognesi, "Synthesis and characterization of benzodithiophene and benzotriazole-based polymers for photovoltaic applications," *Beilstein J. Org. Chem.*, vol. 12, no. 287594, pp. 1629–1637, 2016.

[22] J. L. Banal, J. Subbiah, H. Graham, J. K. Lee, K. P. Ghiggino, and W. W. H. Wong, "Electron deficient conjugated polymers based on benzotriazole," *Polym. Chem.*, vol. 4, no. 4, pp. 1077–1083, 2013.

[23] I. A. Jessop, M. Bustos, and D. Hidalgo, "Synthesis of 2H-benzotriazole based donor-acceptor polymers bearing carbazole derivative as pendant groups: Optical, electronical and photovoltaic properties," *Int. J. Electrochem. Sci.*, vol. 11, no. 12, pp. 9822–9838, 2016.

[24] A. Balan, D. Baran, and L. Toppare, "Benzotriazole containing conjugated polymers for multipurpose organic electronic applications," *Polym. Chem.*, vol. 2, no. 5, pp. 1029–1043, 2011.

[25] S. Yum, T. K. An, and X. Wang, "Benzotriazole-containing planar conjugated polymers with noncovalent conformational locks for thermally stable and efficient polymer field-effect transistors," *Chem. Mater.*, vol. 26, no. 6, pp. 2147–2154, 2014.

[26] J. H. Kim, J. B. Park, and F. Xu, "Effect of π-conjugated bridges of TPD-based medium bandgap conjugated copolymers for efficient tandem organic photovoltaic cells," *Energy Environ. Sci.*, vol. 7, no. 12, pp. 4118–4131, 2014.

[27] Y. Li, "Molecular design of photovoltaic materials for polymer solar cells: Toward suitable electronic energy levels and broad absorption," *Acc. Chem. Res.*, vol. 45, no. 5, pp. 723–733, 2012.

[28] R. Wu, L. Yin, and Y. Li, "π-Linkage effect of push-pull-structure organic small molecules for photovoltaic application," *Sci. China Mater.*, vol. 59, no. 5, pp. 371–388, 2016.

[29] V. Cuesta, M. Vartanian, and P. Malhotra, "Increase in efficiency on using selenophene instead of thiophene in π-bridges for D-π-DPP-π-D organic solar cells," *R. Soc. Chem.*, vol. 7, no. 19, pp. 11886–11894, 2019.

[30] K. A. Singh, E. Sairam, M. Singh, N. Aggarwal, and V. Singhal, *Materials for Electrochromic Devices*, vol. 31, no. April. 2006.

[31] P. M. S. Monk, R. J. Mortimer, and D. R. Rosseinsky, "Electrochromism: Fundamentals and Applications," *J. Am. Chem. Soc.*, vol. 118, no. 7, pp. 1816–1816, 1996.

[32] I. Krull and M. Swartz, "Frequently asked questions about analytical method validation," *Mater. Chem. Phys.*, vol. 16, no. 5, pp. 117–133, 2001.

[33] R. J. Mortimer, "Electrochromic Materials," *Annu. Rev. Mater. Res*, vol. 41, pp. 241–68, 2011.

[34] W. T. Neo, Q. Ye, S. J. Chua, and J. Xu, "Conjugated polymer-based electrochromics: Materials, device fabrication and application prospects," *Am. Chem. Soc.*, vol. 4, no. 31, pp. 7364–7376, 2016.

[35] P. M. S. Monk, R. J. Mortimer, and D. R. Rosseinsky, *Electrochromism and Electrochromic Devices*. 2007.

[36] P. M. S. Monk, *Handbook of Advanced Electronic and Photonic Materials and Devices*, vol. 7. 2001.

[37] P. M. S. Monk, R. J. Mortimer, D. R. Rosseinsky, H. Gerischer, C. W. T. Eds, and J. Wang, *Elctrochromism: Fundamental Applications*. 1995.

[38] K. Bange and T. Gambke, "Electrochromic Materials for optical switching devices," *Adv. Mater.*, vol. 2, no. 1, pp. 10–16, 1990.

[39] L. Lu, T. Zheng, Q. Wu, A. M. Schneider, D. Zhao, and L. Yu, "Recent Advances in Bulk Heterojunction Polymer Solar Cells," *Am. Chem. Soc.*, vol. 115, no. 23, pp. 12666–12731, 2015.

[40] H. Hoppe and N. S. Sariciftci, "Organic solar cells: An overview," *J. Mater.*

Res., vol. 19, no. 7, pp. 1924–1945, 2004.

[41] S. Günes, H. Neugebauer, and N. S. Sariciftci, "Conjugated polymer-based organic solar cells," *Am. Chem. Soc.*, vol. 107, no. 4, pp. 1324–1338, 2007.

[42] M. Hösel, D. Angmo, and F. C. Krebs, *Organic solar cells (OSCs)*. 2013.

[43] A. Gusain, R. M. Faria, and P. B. Miranda, "Polymer solar cells-interfacial processes related to performance issues," *Front. Chem.*, vol. 7, no. February, 2019.

[44] C. Diebel and V. Dyakonov, "Polymer/fullerene bulk heterojunction solar cells," *Reports Prog. Phys.*, vol. 67, no. 1, pp. 5–12, 2019.

[45] O. A. Abdulrazzaq, V. Saini, S. Bourdo, E. Dervishi, and A. S. Biris, "Organic solar cells: A review of materials, limitations, and possibilities for improvement," *Part. Sci. Technol.*, vol. 31, no. 5, pp. 427–442, 2013.

[46] I. Arbouch, Y. Karzazi, and B. Hammouti, "Organic photovoltaic cells: Operating principles, recent developments and current challenges – review," *Phys. Chem. News*, vol. 72, no. 4, pp. 73–84, 2014.

[47] M. Corazza, "Characterization of Organic Solar Cell Devices and their Interfaces under Degradation: Imaging, Electrical and Mechanical Methods," 2016.

[48] S. Rafique, S. M. Abdullah, K. Sulaiman, and M. Iwamoto, "Fundamentals of bulk heterojunction organic solar cells: An overview of stability/degradation issues and strategies for improvement," *Renew. Sustain. Energy Rev.*, vol. 84, no. November 2017, pp. 43–53, 2018.

[49] M. C. Scharber and N. S. Sariciftci, "Efficiency of bulk-heterojunction organic solar cells," *Prog. Polym. Sci.*, vol. 38, no. 12, pp. 1929–1940, 2013.

[50] Y. Huang, E. J. Kramer, A. J. Heeger, and G. C. Bazan, "Bulk heterojunction solar cells: Morphology and performance relationships," *Am. Chem. Soc.*, vol. 114, no. 14, pp. 7006–7043, 2014.

[51] P. Schilinsky, C. Waldauf, and C. J. Brabec, "Recombination and loss analysis in polythiophene based bulk heterojunction photodetectors," *Appl. Phys. Lett.*, vol. 81, no. 20, pp. 3885–3887, 2002.

[52] A. J. Heeger, "25th anniversary article: Bulk heterojunction solar cells: Understanding the mechanism of operation," *Adv. Mater.*, vol. 26, no. 1, pp. 10–28, 2014.

[53] J. M. Nunzi, "Organic photovoltaic materials and devices," *Comptes Rendus Phys.*, vol. 3, no. 4, pp. 523–542, 2002.

[54] K. Anagnostou, M. M. Stylianakis, K. Petridis, and E. Kymakis, "Building an

organic solar cell: Fundamental procedures for device fabrication," *MDPI*, vol. 12, no. 11, 2019.

[55] M. E. Ragoussi and T. Torres, "New generation solar cells: Concepts, trends and perspectives," *Chem. Commun.*, vol. 51, no. 19, pp. 3957–3972, 2015.

[56] J. Xue, S. Uchida, B. P. Rand, and S. R. Forrest, "4.2% Efficient Organic Photovoltaic Cells With Low Series Resistances," *Appl. Phys. Lett.*, vol. 84, no. 16, pp. 3013–3015, 2004.

[57] C. J. Brabec, A. Cravino, D. Meissner, and N. S. Sariciftci, "The influence of materials work function on the open circuit voltage of plastic solar cells," *Thin Solid Films*, vol. 403–404, pp. 368–372, 2002.

[58] M. Zhang, H. Wang, and C. W. Tang, "Effect of the highest occupied molecular orbital energy level offset on organic heterojunction photovoltaic cells," *Appl. Phys. Lett.*, vol. 97, no. 14, pp. 1–4, 2010.

[59] S. Almosni, A. Delamarre, and Z. Jehl, "Material challenges for solar cells in the twenty-first century: directions in emerging technologies," *Sci. Technol. Adv. Mater.*, vol. 19, no. 1, pp. 336–369, 2018.

[60] M. Jørgensen, K. Norrman, S. A. Gevorgyan, T. Tromholt, B. Andreasen, and F. C. Krebs, "Stability of polymer solar cells," *Adv. Mater.*, vol. 24, no. 5, pp. 580–612, 2012.

[61] J. M. Kroon, M. M. Wienk, W. J. H. Verhees, and J. C. Hummelen, "Accurate efficiency determination and stability studies of conjugated polymer/fullerene solar cells," *Thin Solid Films*, vol. 403–404, pp. 223–228, 2002.

[62] G. Yu, J. Gao, J. C. Hummelen, F. Wudl, and A. J. Heeger, "Polymer photovoltaic cells: Enhanced efficiencies via a network of internal donor-acceptor heterojunctions," *Science (80-.).*, vol. 270, no. 5243, p. 1789, 1995.

[63] Y. Terao, H. Sasabe, and C. Adachi, "Correlation of hole mobility, exciton diffusion length, and solar cell characteristics in phthalocyanine/fullerene organic solar cells," *Appl. Phys. Lett.*, vol. 90, no. 10, 2007.

[64] S. B. Rim, R. F. Fink, J. C. Schöneboom, P. Erk, and P. Peumans, "Effect of molecular packing on the exciton diffusion length in organic solar cells," *Appl. Phys. Lett.*, vol. 91, no. 17, 2007.

[65] K. H. Park, Y. J. Kim, and G. B. Lee, "Recently Advanced Polymer Materials Containing Dithieno[3,2-b:2′,3′-d]phosphole Oxide for Efficient Charge Transfer in High-Performance Solar Cells," *Adv. Funct. Mater.*, vol. 25, no. 26, pp. 3991–3997, 2015.

[66] H. Hwang, D. H. Sin, and C. Kulshreshtha, "Synergistic effects of an alkylthieno[3,2-: B] thiophene π-bridging backbone extension on the

photovoltaic performances of donor-acceptor copolymers," *J. Mater. Chem. A*, vol. 5, no. 21, pp. 10269–10279, 2017.

[67] S. C. Price, A. C. Stuart, L. Yang, H. Zhou, and W. You, "Fluorine substituted conjugated polymer of medium band gap yields 7% efficiency in polymer-fullerene solar cells," *J. Am. Chem. Soc.*, vol. 133, no. 12, pp. 4625–4631, 2011.

[68] J. M. Jiang, P. A. Yang, H. C. Chen, and K. H. Wei, "Synthesis, characterization, and photovoltaic properties of a low-bandgap copolymer based on 2,1,3-benzooxadiazole," *Chem. Commun.*, vol. 47, no. 31, pp. 8877–8879, 2011.

[69] G. Hizalan, A. Balan, D. Baran, and L. Toppare, "Spray processable ambipolar benzotriazole bearing electrochromic polymers with multi-colored and transmissive states," *J. Mater. Chem.*, vol. 21, no. 6, pp. 1804–1809, 2011.

[70] M. Yuan, P. Yang, M. M. Durban, and C. K. Luscombe, "Low bandgap polymers based on silafluorene containing multifused heptacylic arenes for photovoltaic applications," *Macromolecules*, vol. 45, no. 15, pp. 5934–5940, 2012.

[71] I. Onk, G. Hizalan, S. C. Cevher, S. O. Hacioglu, L. Toppare, and A. Cirpan, "Multipurpose selenophene containing conjugated polymers for optoelectronic applications," *J. Macromol. Sci. Part A Pure Appl. Chem.*, vol. 54, no. 3, pp. 133–139, 2017.

[72] V. Cuesta, M. Vartanian, and P. Malhotra, "Increase in efficiency on using selenophene instead of thiophene in π-bridges for D-π-DPP-π-D organic solar cells," *J. Mater. Chem. A*, vol. 7, no. 19, pp. 11886–11894, 2019.

[73] R. Kroon, M. Lenes, J. C. Hummelen, P. W. M. Blom, and B. De Boer, "Small bandgap polymers for organic solar cells (polymer material development in the last 5 years)," *Polym. Rev.*, vol. 48, no. 3, pp. 531–582, 2008.

[74] A. Patra and M. Bendikov, "Polyselenophenes," *J. Mater. Chem.*, vol. 20, no. 3, pp. 422–433, 2010.

[75] H. Y. Chen, S. C. Yeh, C. T. Chen, and C. T. Chen, "Comparison of thiophene- and selenophene-bridged donor-acceptor low band-gap copolymers used in bulk-heterojunction organic photovoltaics," *J. Mater. Chem.*, vol. 22, no. 40, pp. 21549–21559, 2012.

[76] A. A. B. Alghamdi, D. C. Watters, and H. Yi, "Selenophene vs. thiophene in benzothiadiazole-based low energy gap donor-acceptor polymers for photovoltaic applications," *J. Mater. Chem. A*, vol. 1, no. 16, pp. 5165–5171, 2013.

[77] M. Shahid, R. S. Ashraf, and Z. Huang, "Photovoltaic and field effect transistor performance of selenophene and thiophene diketopyrrolopyrrole co-polymers

with dithienothiophene," *J. Mater. Chem.*, vol. 22, no. 25, pp. 12817–12823, 2012.

[78] J. Y. Kim, "Effect of solvents on the electrical and morphological characteristics of polymer solar cells," *Polymers (Basel).*, vol. 11, no. 2, 2019.

[79] B. Y. Kadem, A. K. Hassan, and W. Cranton, "The effects of organic solvents and their co-solvents on the optical, structural, morphological of P3HT:PCBM organic solar cells," *AIP Conf. Proc.*, vol. 1758, no. 2016, 2016.

[80] C. Duan, Z. Peng, and F. J. M. Colberts, "Efficient Thick-Film Polymer Solar Cells with Enhanced Fill Factors via Increased Fullerene Loading," *ACS Appl. Mater. Interfaces*, vol. 11, no. 11, pp. 10794–10800, 2019.

APPENDICES

A. NMR DATA

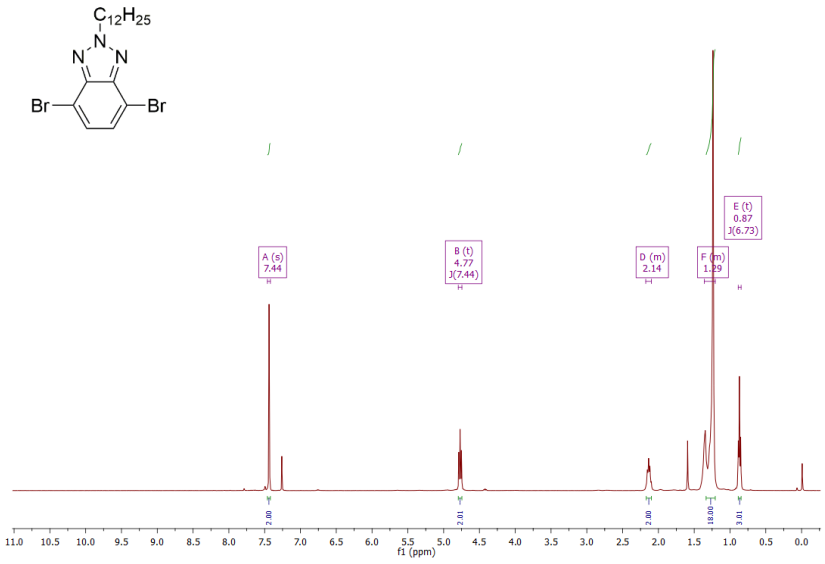

Figure A. 1. ^{1}H spectrum of 4,7-dibromo-2-dodecyl-2H-benzo[d][1,2,3]triazole

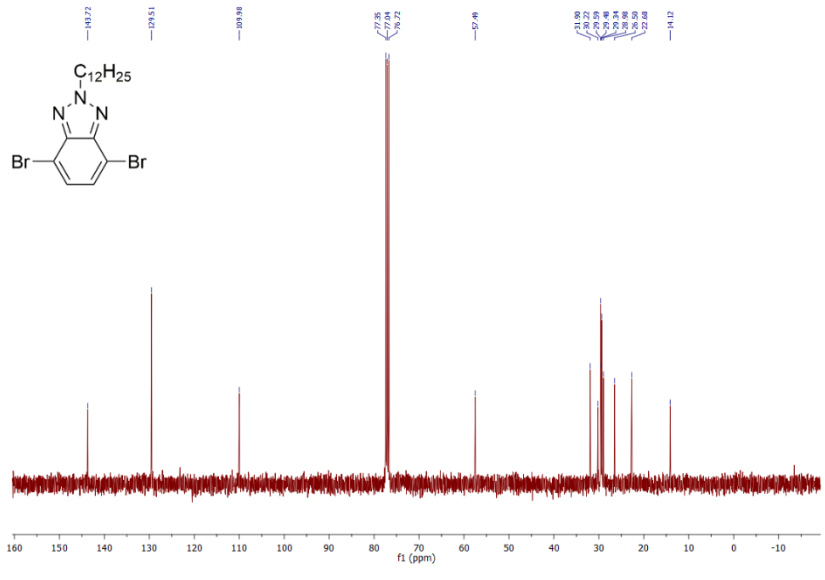

Figure A. 2. ^{13}C spectrum of 4,7-dibromo-2-dodecyl-2H-benzo[d][1,2,3]triazole

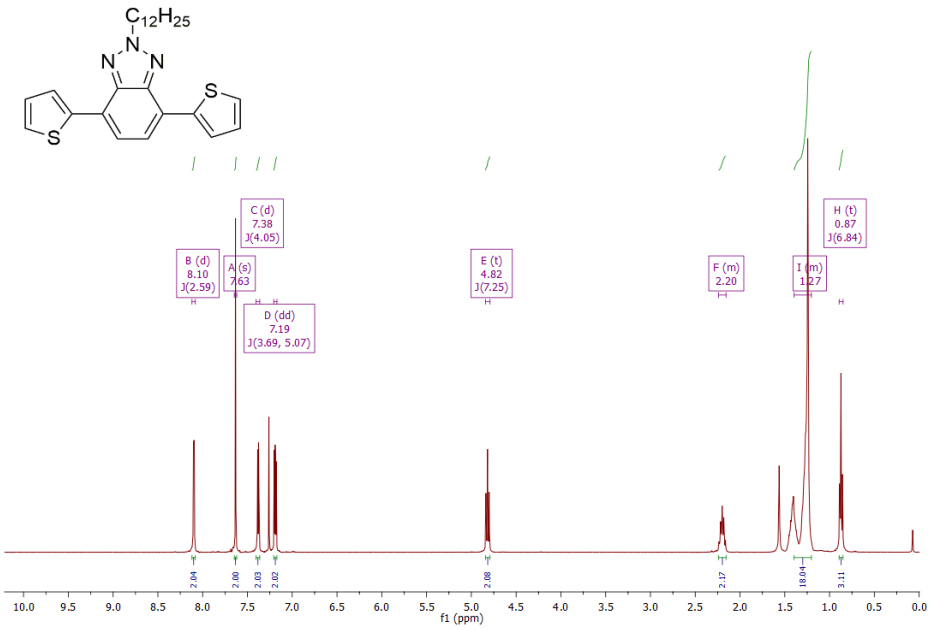

Figure A. 3. ^{1}H spectrum of 2-dodecyl-4,7-di(thiophen-2-yl)-2H-benzo[d][1,2,3]triazole

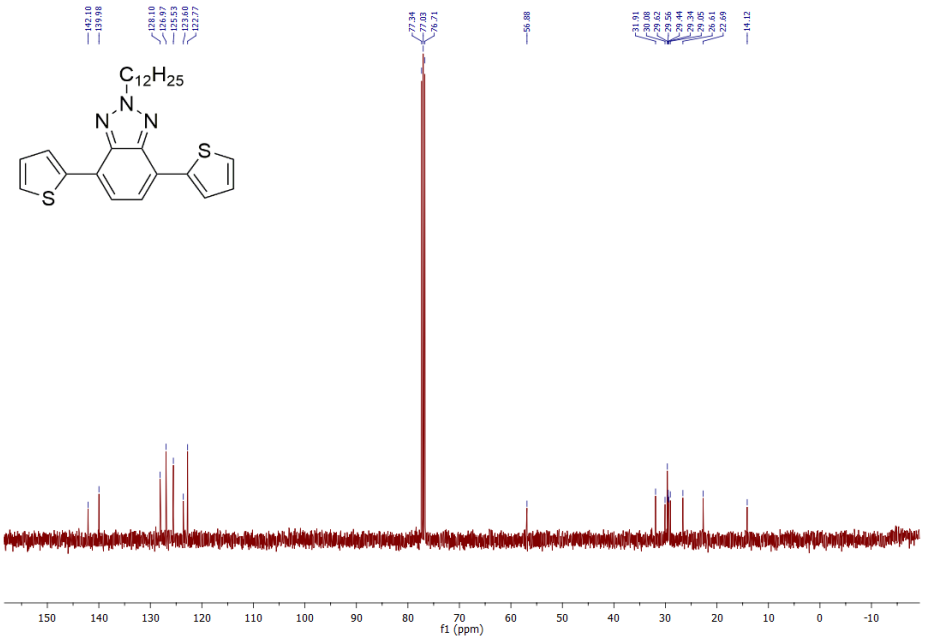

Figure A. 4. ^{13}C spectrum of 2-dodecyl-4,7-di(thiophen-2-yl)-2H-benzo[d][1,2,3]triazole

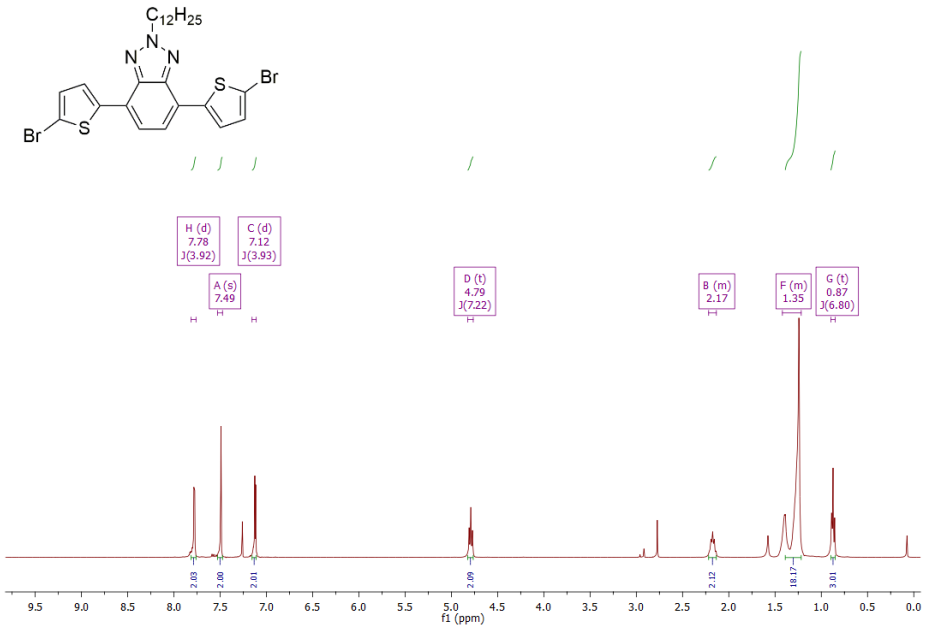

Figure A. 5. ^{1}H spectrum of 4,7-bis(5-bromothiophen-2-yl)-2-dodecyl-2H-benzo[d][1,2,3] triazole

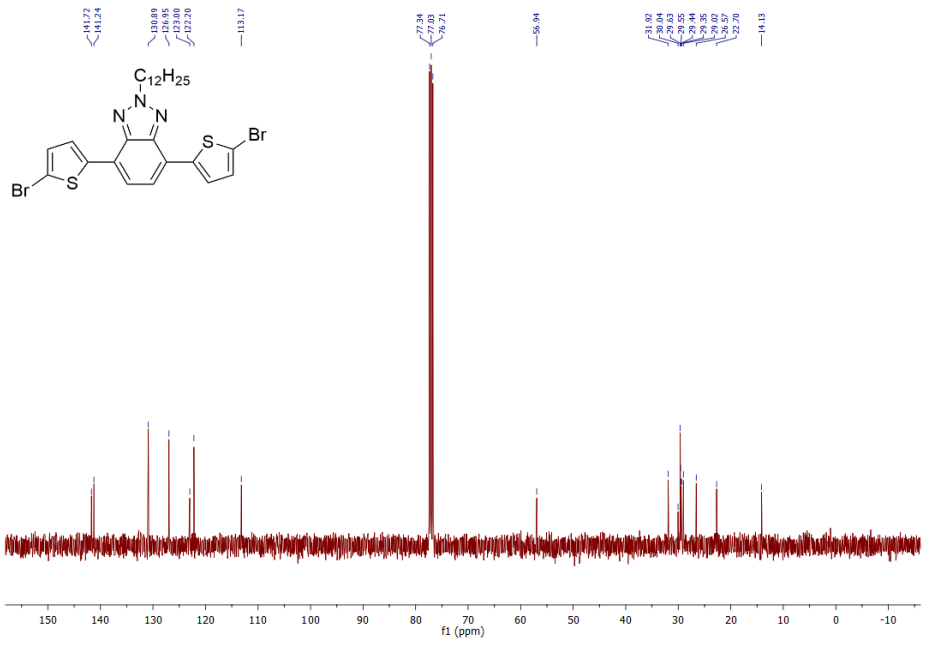

Figure A. 6. ^{13}C spectrum of 4,7-bis(5-bromothiophen-2-yl)-2-dodecyl-2H-benzo[d][1,2,3] triazole

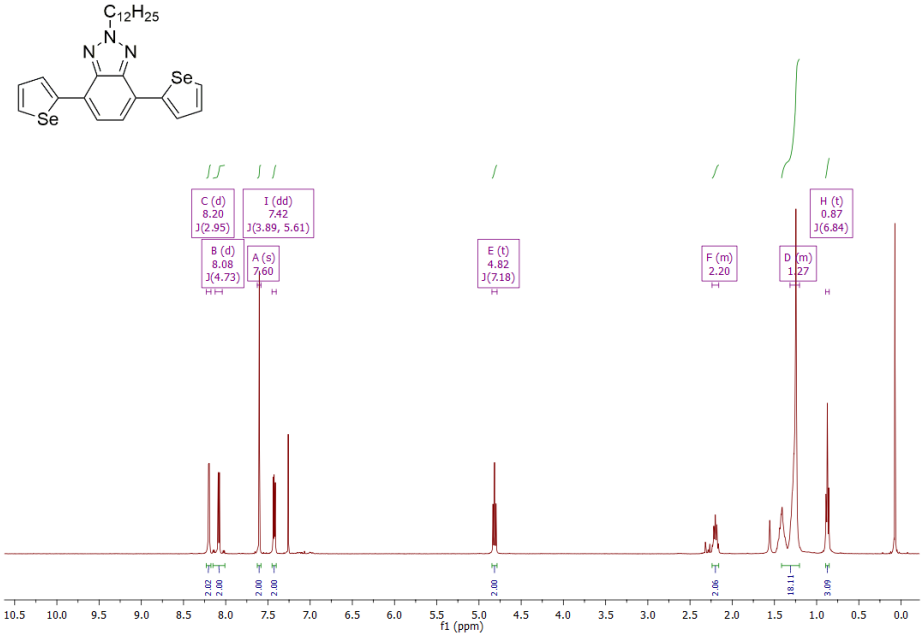

Figure A. 7. ^{1}H spectrum of 2-dodecyl-4,7-di(selenophen-2-yl)-2H-benzo[d][1,2,3]triazole

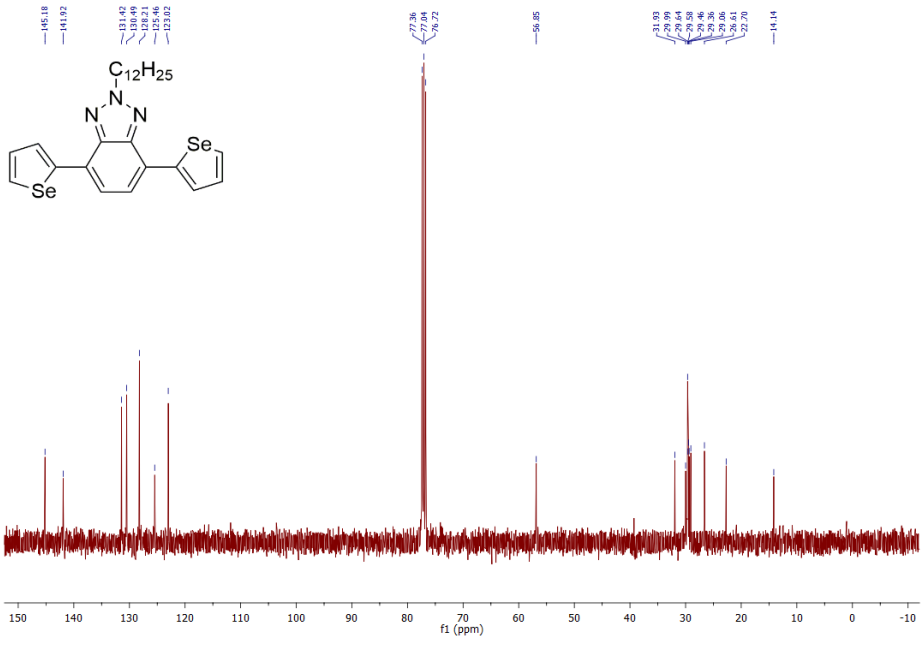

Figure A. 8. ^{13}C spectrum of 2-dodecyl-4,7-di(selenophen-2-yl)-2H-benzo[d][1,2,3]triazole

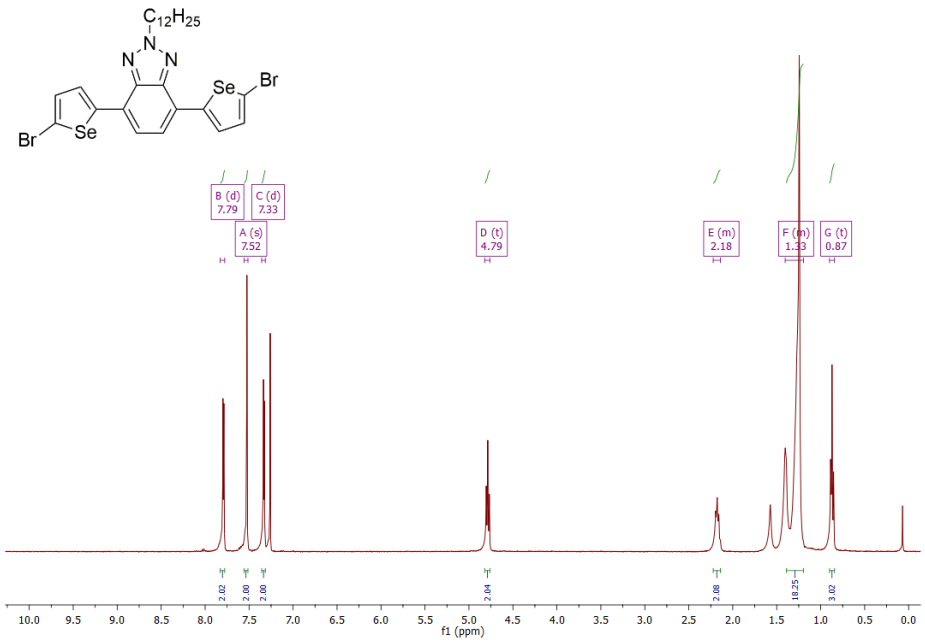

Figure A. 9. ^{1}H spectrum of 4,7-bis(5-bromoselenophen-2-yl)-2-dodecyl-2H-benzo[d][1,2,3]triazole

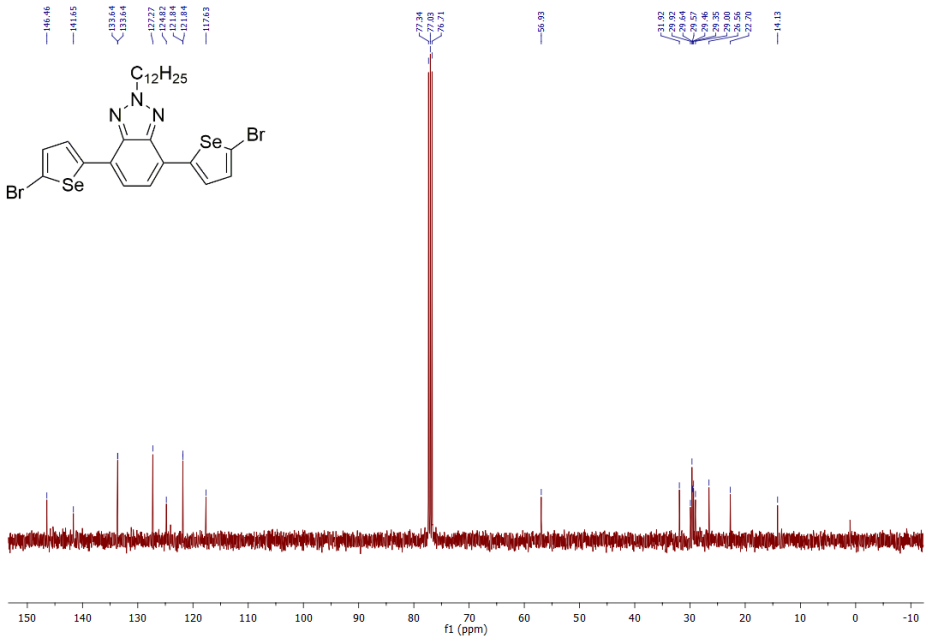

Figure A. 10. ^{13}C spectrum of 4,7-bis(5-bromoselenophen-2-yl)-2-dodecyl-2H-benzo[d][1,2,3]triazole

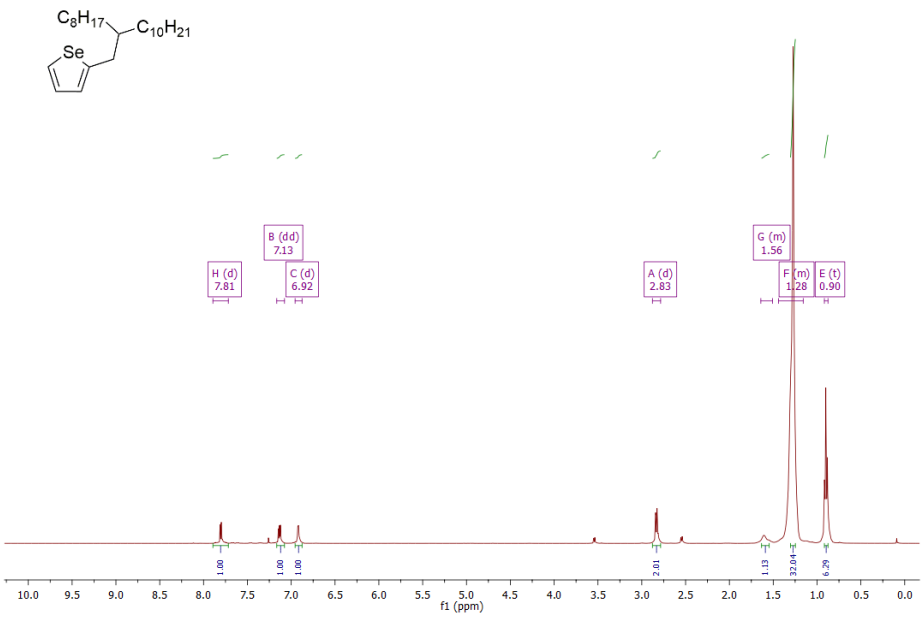

Figure A. 11. ^{1}H spectrum of 2-(2-octyldodecyl)selenophene

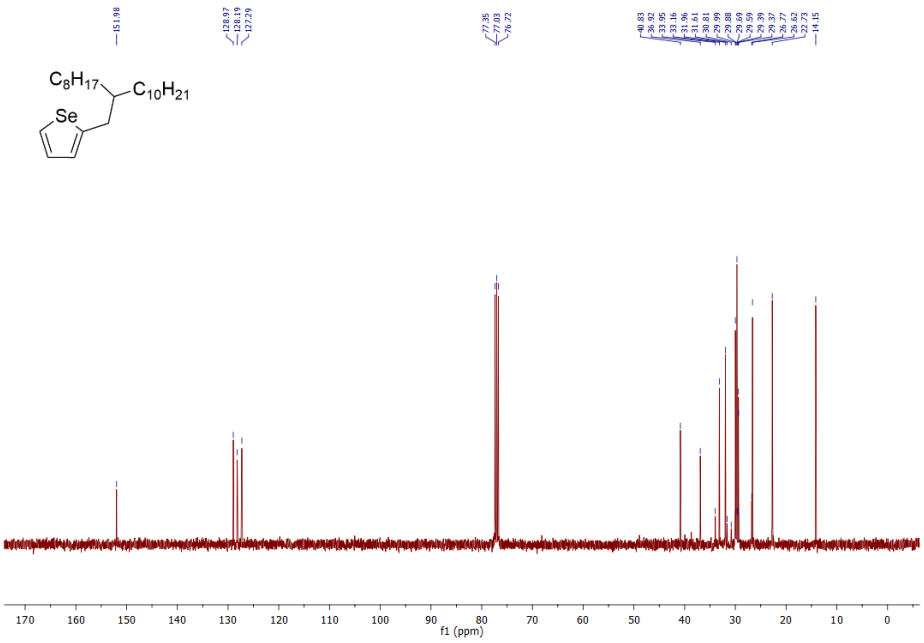

Figure A. 12. ^{13}C spectrum of 2-(2-octyldodecyl)selenophene

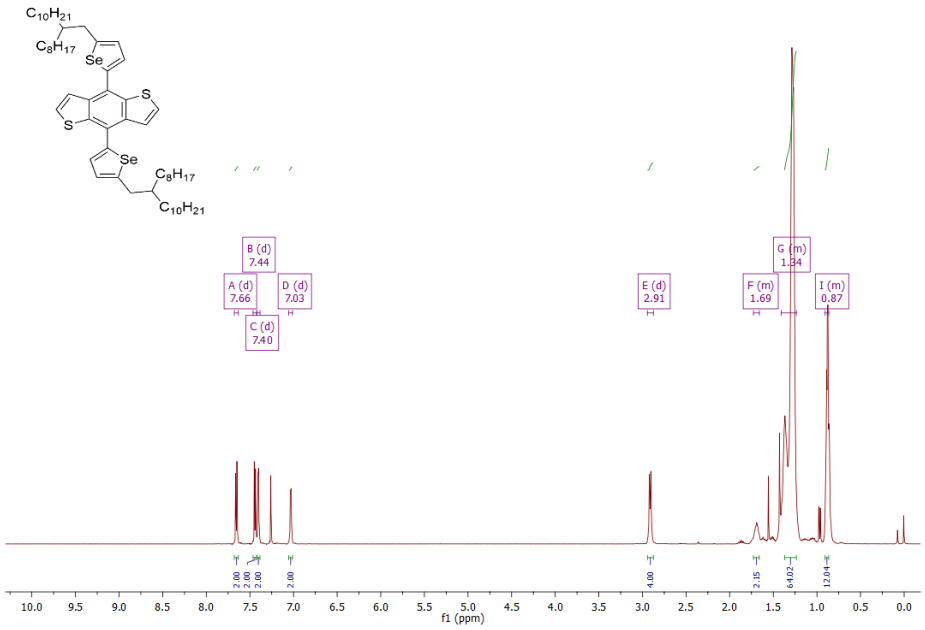

Figure A. 13. ^{1}H spectrum of 4,8-bis(5-(2-octyldodecyl)selenophen-2-yl)benzo[1,2-b:4,5-b']dithiophene

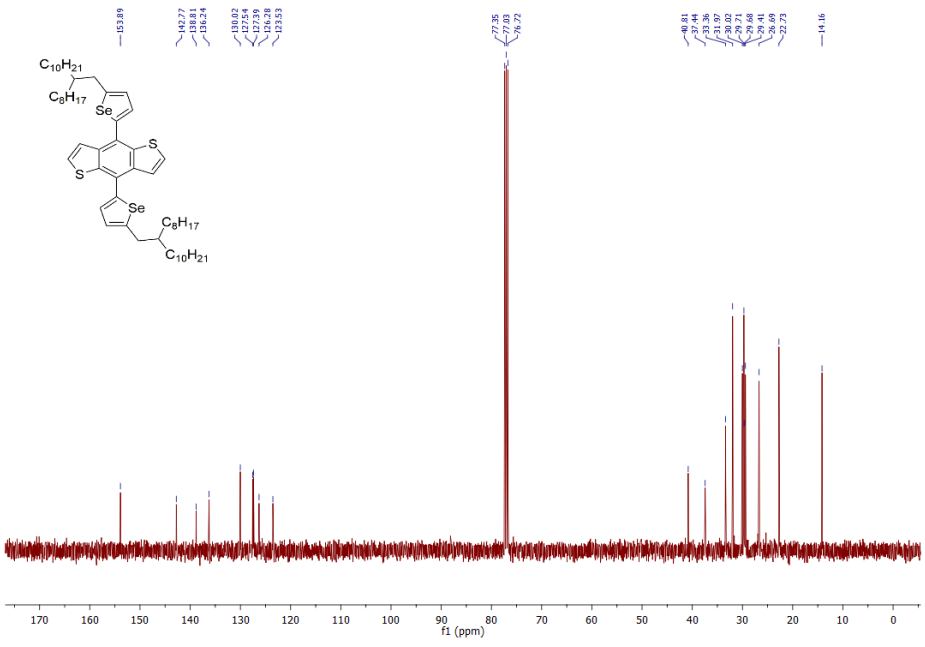

Figure A. 14. ^{13}C spectrum of 4,8-bis(5-(2-octyldodecyl)selenophen-2-yl)benzo[1,2-b:4,5-b']dithiophene

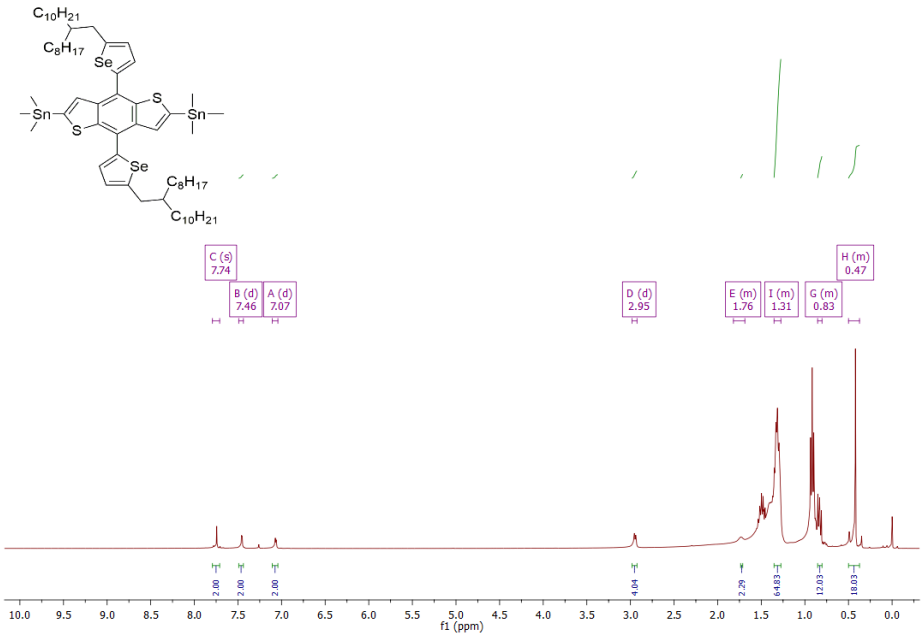

Figure A. 15. ^{1}H spectrum of (4,8-bis(5-(2-octyldodecyl) selenophen-2-yl)benzo[1,2-b:4,5-b']dithiophene-2,6-diyl)bis(trimethylstannane)

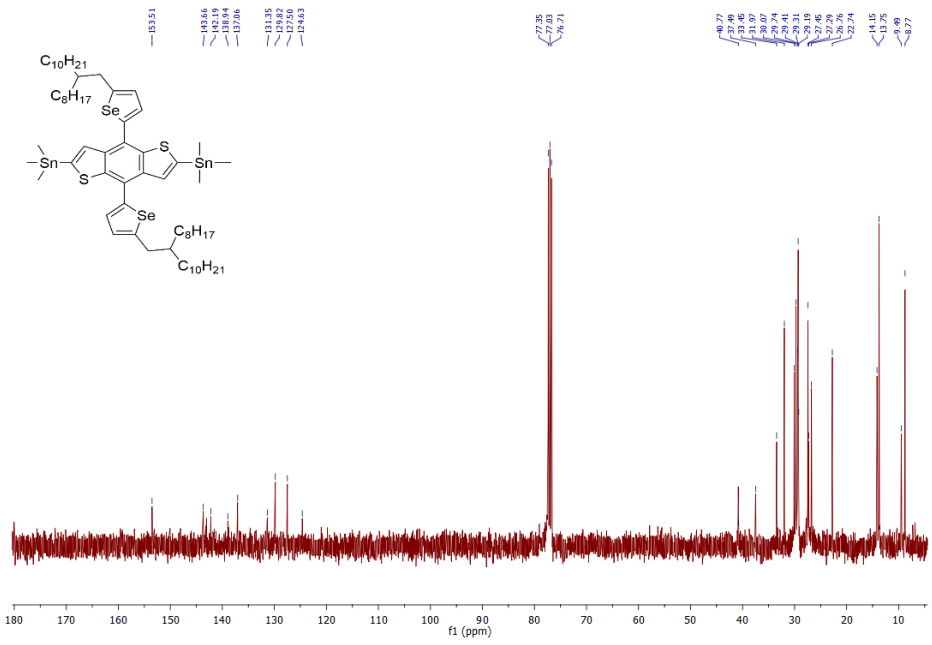

Figure A. 16. ^{13}C spectrum of (4,8-bis(5-(2-octyldodecyl) selenophen-2-yl)benzo[1,2-b:4,5-b']dithiophene-2,6-diyl)bis(trimethylstannane)

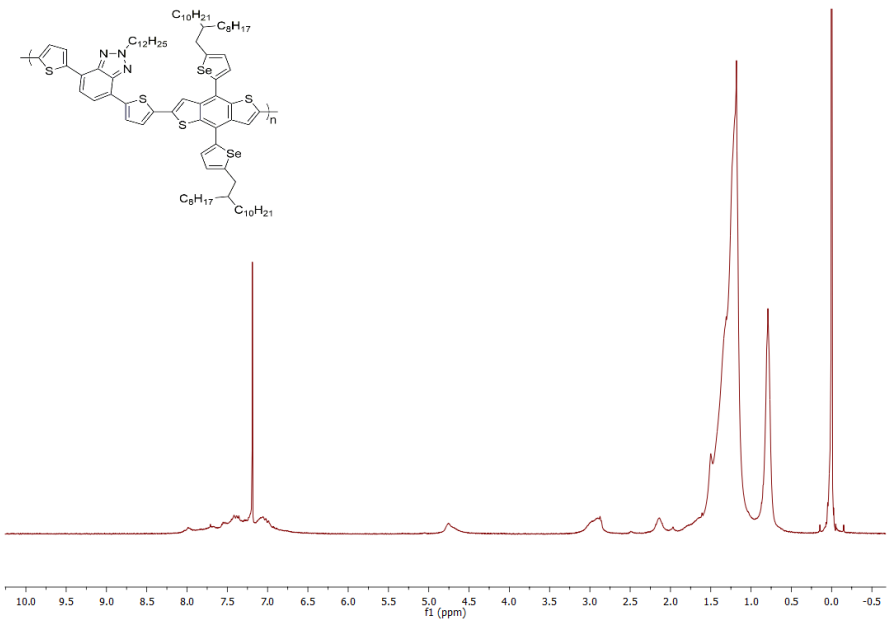

Figure A. 17. ^{1}H spectrum of P1

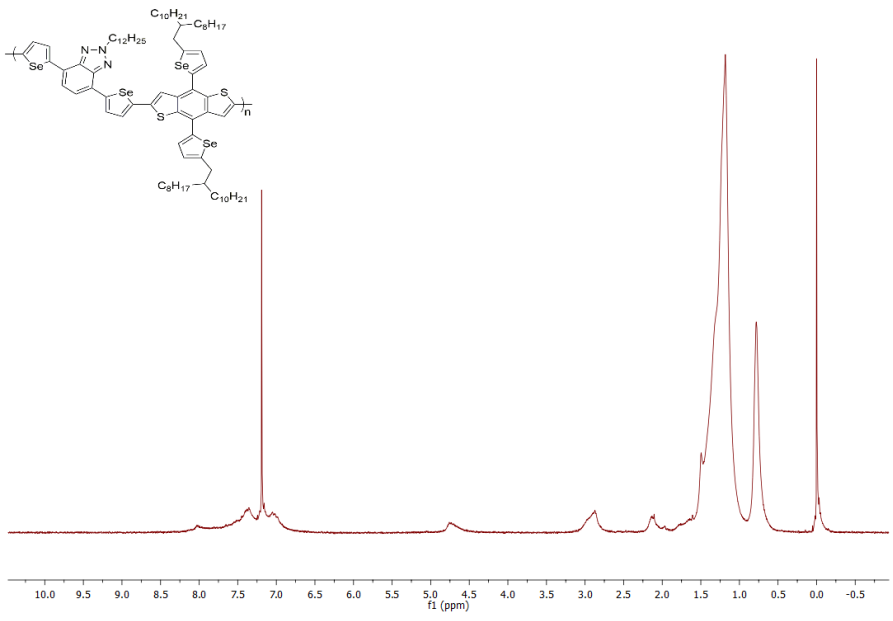

Figure A. 18. ^{1}H spectrum of P2

B. THERMAL ANALYSIS RESULTS

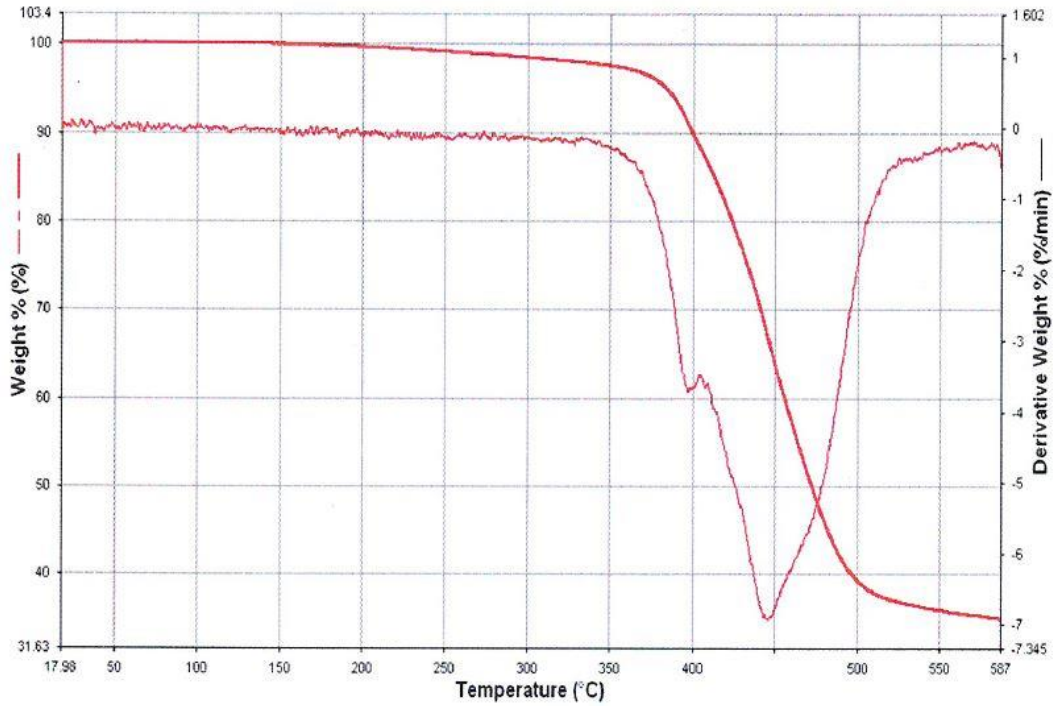

Figure B. 1. TGA Thermogram of P1

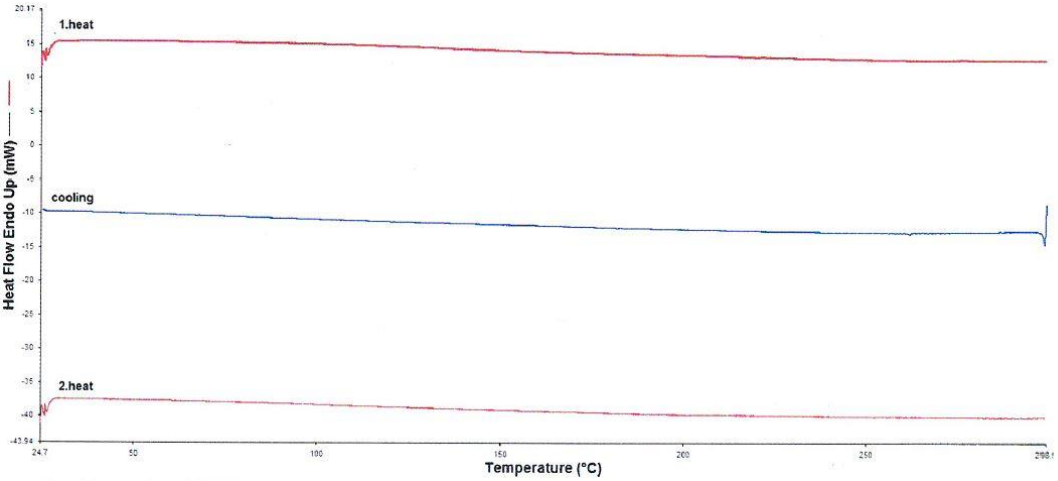

Figure B. 2. DSC Curve of P1

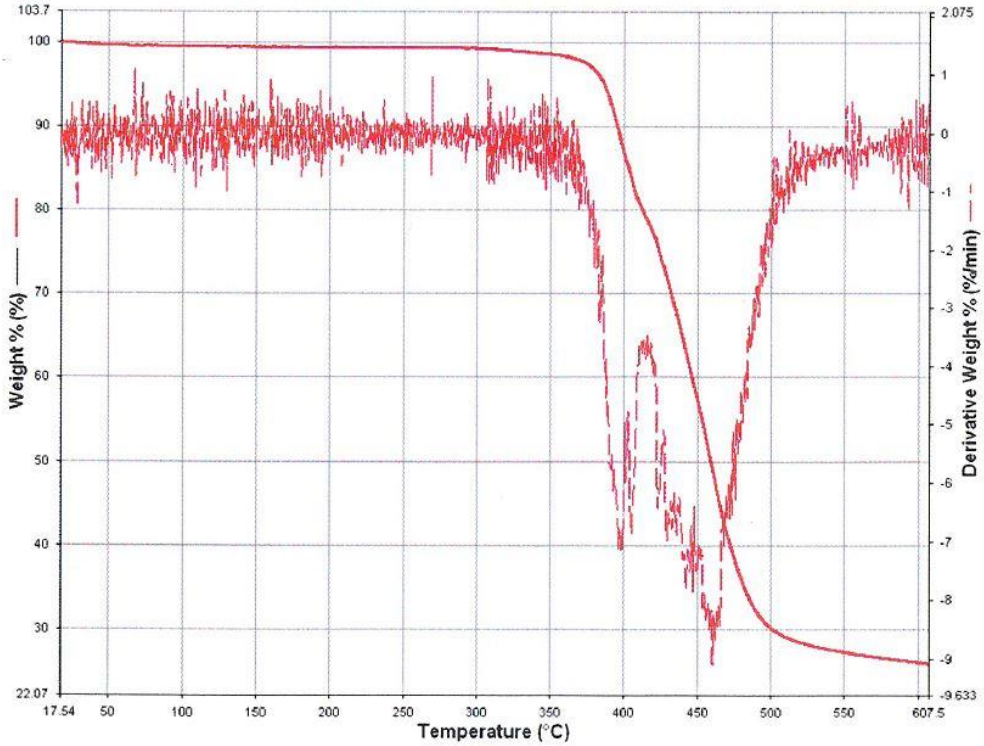

Figure B. 3. TGA Thermogram of P2

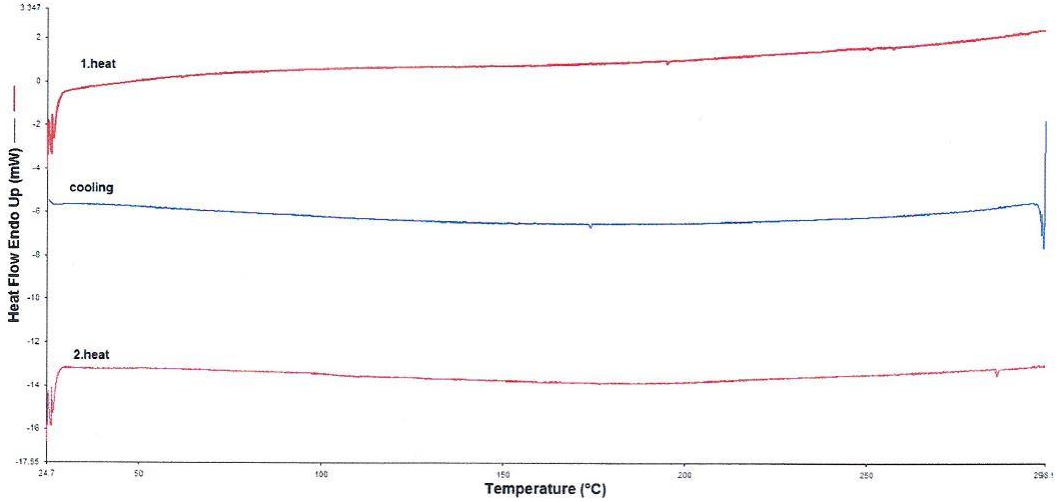

Figure B. 4. DSC Curve of P2